agso RESEARCH NEWSLETTER

'Geoscience for Australia's Future'

Number 31 November 1999

Finding new mineral prospects with HYMAP: early results from a hyperspectral remote-sensing case study in the west Pilbara

Phil Bierwirth[1], Richard Blewett[2], & David Huston[2]

New research conducted in the Pilbara region of Western Australia has demonstrated that high-resolution remote sensing can detect minerals associated with ore deposits. The flat terrain, sparse exposure, and weathering and 'calcretisation' of bedrock in this area hamper the visual identification of hydrothermal alteration minerals. HYMAP (airborne hyperspectral remote sensing) is a rapid and cost-effective exploration tool that provides valuable new information on the geology and the distribution of surface minerals.

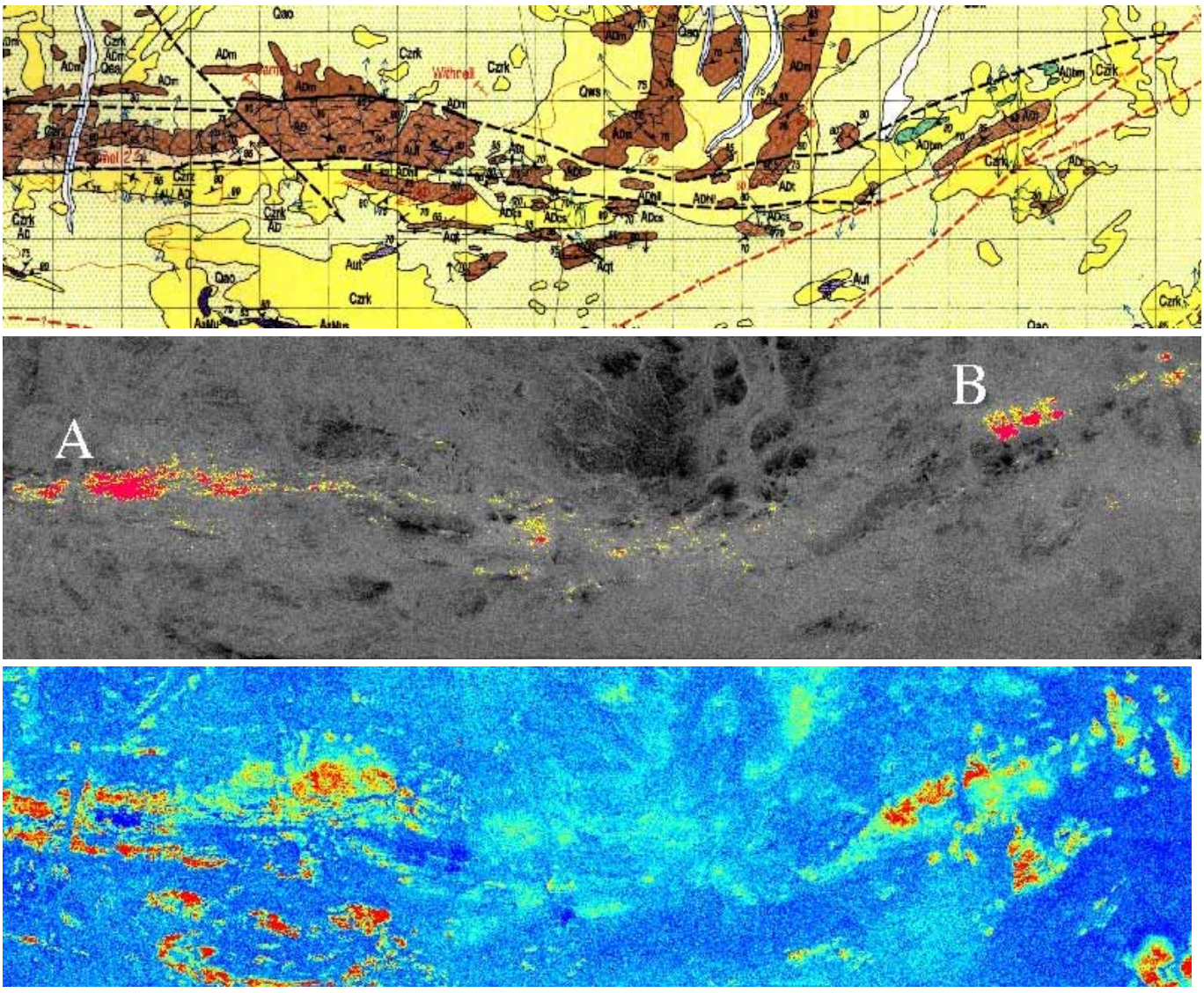

Fig. 1. An 18 × 5-km area of the Indee district, in the Yule 1:100 000 Sheet area. *(a)* Geology (from Smithies 1998: op. cit.): brown (Adm), metasediments of the Archaean Mallina Formation; green (Adbm) and purple (Aut), mafic to ultramafic igneous rocks; bright yellow (Czrk), calcrete; pale yellow (Qac), sand; the dashed and solid black lines distinguish the Mallina Fault Zone; the red dashed lines represent magnetic lineaments. *(b)* Pyrophyllite abundance image derived from mixture-modelling of the airborne HYMAP data: red reflects high concentrations of pyrophyllite; yellow, low but detectable concentrations of pyrophyllite. *(c)* Dolomite abundance image derived from mixture-modelling of the airborne HYMAP data: red reflects high concentrations of dolomite; yellow and green, lower concentrations; blue, no detectable dolomite.

Contents: inside on p. 2

AGSO

Australian Geological Survey Organisation

a research organisation of the Department of Industry, Science & Resources

Survey area and HYMAP data acquisition

As part of the joint AGSO–GSWA 'North Pilbara' project for the National Geoscience Mapping Accord, an aircraft carrying the hyperspectral HYMAP system (Cocks et al. 1998: 'First EARSEL Workshop on Imaging Spectrometry', University of Zurich, October, 1998) surveyed an area of ~180 km² in the west Pilbara. The survey area covered the Indee district, where Resolute Ltd recently discovered zones of gold mineralisation.

The regional geology (Smithies 1998: 'Geology of the Yule 1:100 000 Sheet', Geological Survey of Western Australia) comprises Archaean Mallina Formation metasediments deformed by the east-striking Mallina Shear Zone (Fig. 1a). An extensive shallow cover of residual sand and calcrete regolith (Figs. 1a and 2) largely conceals outcrop. The gold occurs in a variety of styles associated with hydrothermal quartz veins and breccias with distinctive alteration mineral assemblages.

The HYMAP sensor collects reflected solar radiation in 128 bands covering the 0.44–2.5-μm wavelength range, which includes the visible, near infra-red, and short-wave infra-red regions of the electromagnetic spectrum. For an image pixel size of ~10 × 10 m, our survey sampled a spectrum for every pixel in the area. Each spectrum is a mixture of spectral components — including vegetation and minerals, and atmospheric and illumination effects. Our analysis of the HYMAP data incorporated an atmospheric correction, and modelling of the various component mixtures to produce mineral abundance maps.

HYMAP data presentation, verification, and interpretation

Figure 1b, generated by mixture-modelling of HYMAP data, shows a number of 'bullseye' targets of pyrophyllite distributed along the Mallina Shear Zone, notably areas A and B. Pyrophyllite is a high-temperature hydrothermal mineral and is closely associated with certain styles of gold mineralisation. Pyrophyllite in high abundance (red) at target A is spatially adjacent to an extensively drilled gold prospect returning gold assays >10 m @ ~7–11 g/t (Gold Gazette, November 1998, p. 5). Along strike, target area B (Fig. 2) has been regionally explored only, and, according to the intensity of the pyrophyllite association, represents a new prospect.

Fig. 2. Sand- and spinifex-covered landscape at target area B.

A comparison of spectral signatures of pure pyrophyllite and the spectrum measured by the HYMAP data clearly shows a characteristic absorption feature at 2.167 μm (Fig. 3). Ground-checking samples in target areas A and B with a Portable Infrared Mineral Analyser (PIMA) confirmed the presence of pyrophyllite (Fig. 3).

Comparison of the pyrophyllite image (Fig. 1b) with the geology (Fig. 1a) shows that the new prospect (area B) is partly covered by calcrete and sand (cf. Fig. 2). The target area is flat, largely free of outcrop, and strewn with lag. Here, the pyrophyllite occurrence coincides with the location of the shear zone, and

In this issue

may reflect an along-strike continuation of mineralisation. Assay results on a hand specimen from area B returned anomalous gold (0.34 ppm), confirming the prospectivity of the HYMAP-identified target. PIMA spectral analysis of field samples targeted by the image map identified the carbonate in the calcrete as mainly dolomite (cf. Fig. 1c). Whereas the dolomite image map (Fig. 1c) generally corresponds closely with the mapped geology (Fig. 1a), some areas of calcrete cover have been somewhat generalised on the 1:100 000 geological map, so the image shows a more precise distribution and subdivision of dolomite-bearing calcrete regolith.

Dolomite reflectance curves (Fig. 4) reveal a broad carbonate absorption feature centred at about 2.33 μm in the pure laboratory sample and in the PIMA spectrum of a sample obtained in the field. This feature is also evident in the dolomite pixel in the HYMAP data, but only as a low broad feature. The low reflectance in the HYMAP data beyond 2.35 μm may be due to a problem with the initial conversion of the data to reflectance. This problem of low HYMAP reflectance in this part of the spectrum affects all pixels, and will have to be resolved. However, the mixture-modelling analysis was able to detect the relative influence of the broad feature in the HYMAP spectrum shown in Figure 4.

Conclusions

The preliminary results presented here demonstrate the ability of hyperspectral remote sensing to detect mineral deposits in areas of shallow, residual regolith cover. Thus, the HYMAP identification of the alteration mineral, pyrophyllite (a known associate of gold), defines new exploration targets (which were subsequently confirmed by assay results). Imaging of dolomite abundance, confirmed by PIMA ground-checking, helps to identify groundwater-deposited materials and associations with carbonate alteration in mineralised zones.

Alteration minerals were recognised in this study despite the area's regolith problems such as flat terrain, sparse exposure, 'calcretisation', and extensive bedrock weathering. This is particularly exciting, as HYMAP might be a suitable exploration tool in other prospective areas evincing a similar regolith history (e.g., shallow residual cover).

The accurate, rapid, and cost-effective identification of alteration minerals as vectors to ore (as detected by HYMAP) in this area is largely beyond the geologist in the field. To date, such alteration-mineral identification has applied extensive and time-consuming laboratory work on samples by non-spectral methods.

Although not presented here, HYMAP has successfully identified other hydrothermal alteration minerals (such as sericite, chlorite, kaolinite, calcite, etc.). Analysis of these and other mineral combinations reveals additional geological information not readily acquired from other, traditional mapping techniques.

[1] Department of Geology, Australian National University, Canberra, ACT; email philb@geology.anu.edu.au.

[2] Minerals Division, Australian Geological Survey Organisation, GPO Box 378, Canberra, ACT, 2601; tel. +61 2 6249 9713 (RB), +61 2 62499577 (DH), fax +61 2 6249 9983; email richard.blewett@agso.gov.au, david.huston@agso.gov.au.

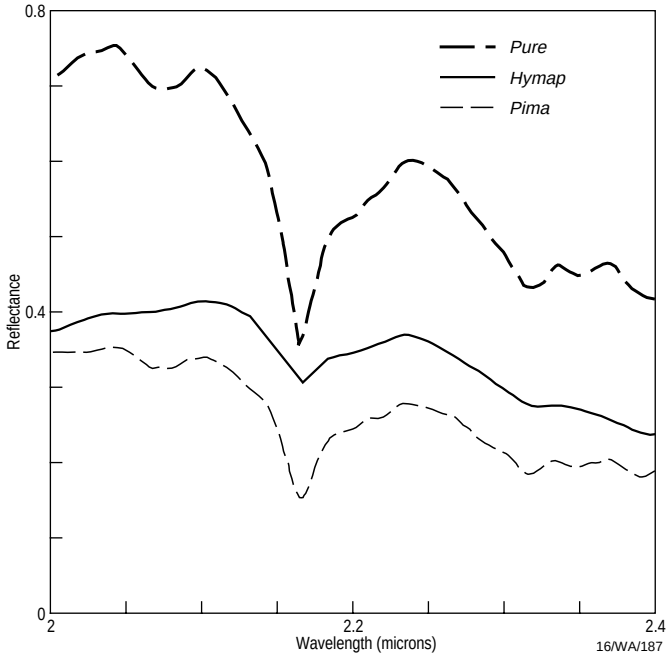

Fig. 3. Pyrophyllite reflectance curves for a pure sample measured in the laboratory, a pyrophyllite-rich pixel measured by HYMAP, and PIMA analysis of a field sample.

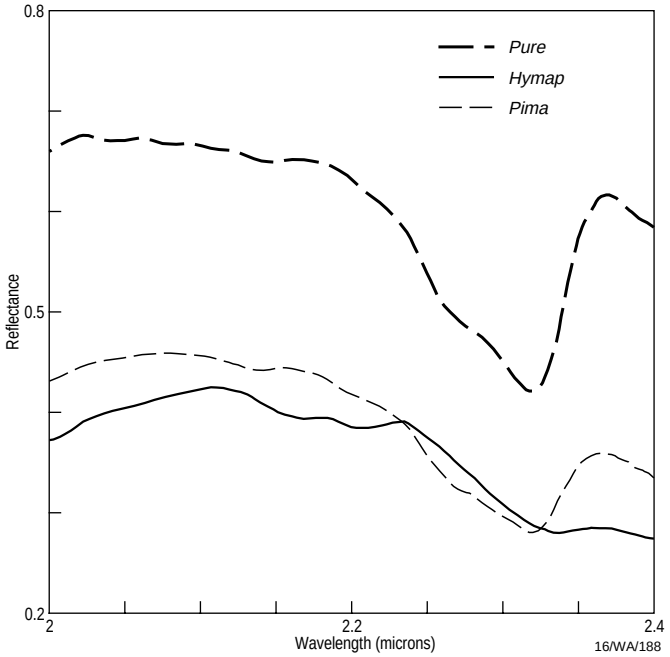

Fig. 4. Dolomite reflectance curves for a pure sample measured in the laboratory, a dolomite-rich pixel measured by HYMAP, and PIMA analysis of a field sample.

Nutrient recycling and benthic activity in a shallow coastal lagoon in Western Australia

David J. Fredericks[1], David T. Heggie[1], Andrew Longmore[2], Duncan Palmer[1], Craig Smith[1], & Graham W.S. Skyring[3]

A collaborative study of benthic activity in Wilson Inlet (southwest WA; Fig. 5) has found that nitrogen released as ammonium contributes to high NH_4^+ fluxes, which are considerably reduced by microphytobenthos (MPB, small bottom-dwelling algae) in summer and autumn. The benthic fluxes of NH_4^+ are higher than the catchment fluxes, and can be sustained only by rapid recycling of nitrogen from the sea-floor.

The study contributed to an assessment of the capacity of Wilson Inlet, a recreational reserve, to accommodate nutrient and sediment discharge from the catchment, and local point sources of discharge (such as sewerage treatment plants).

Study site

Wilson Inlet is a coastal lagoon ~14 km long by 4 km wide with an average depth of 1.7 m. It comprises a distinct marine-sand delta opening into a central basin up to 4.5 m deep underlain by organic-rich mud (up to 9% organic carbon). Coarse, probably fluviodeltaic sand is accumulating at the estuary perimeter and river entrances.

The Inlet has a highly seasonal run-off, reflecting the Mediterranean-type climate (hot dry summers, cool wet winters): most rainfall occurs in winter, virtually none in summer. It is isolated from the sea by a sand bar for ~7 months a year (usually January–August), but is tidal while open to the sea. Tides in the Inlet (<10 cm) are considerably more attenuated than marine tides (1.2 m), and sea-level changes due to atmospheric effects commonly exert a greater influence on sea-water exchange than astronomic tides (Lukatelich et al. 1987: Estuarine, Coastal and Shelf Science, 24, 141–165). Accordingly, marine water entering the Inlet settles to form a generally shallow (<0.5-m-thick) layer of bottom water.

Nutrient (N and P) and chlorophyll-a concentrations in the Inlet are generally low. Even so, the bulk of the bottom of the Inlet lies within the photic zone in summer, which has favoured the proliferation of a large MPB community.

Materials and methods

Using benthic chambers and techniques described in Berelson et al. 1996 (AGSO Record 1996/17), we measured benthic fluxes in situ at four sites (6, 12, 18 and 30; Fig. 5) in the mud facies in spring (November 1997), summer (February 1999), autumn (May 1998) and winter–early spring when run-off is still occurring (September 1998). The Inlet was isolated from the sea and the water column well mixed during the autumn survey, and stratified during the other surveys.

Most parameters were measured in chambers that isolated ~7 L of water above the bottom sediment. Two transparent chambers and two opaque chambers were deployed at each site with a central data logger that recorded the concentration of dissolved oxygen and temperature in each chamber and in ambient bottom water.

Dissolved oxygen within the chamber was measured every 5 min by a pulsed electrode. Five 100-mL samples withdrawn from the chambers during a 6-hour deployment were immediately filtered and analysed in an onshore laboratory. Two chambers equipped with conductivity–temperature–depth probes automatically collected samples for analysis at pre-programmed intervals in additional deployments.

Nitrite (NO_2–N), nitrate (NO_3–N), ammonia (NH_4^+–N), orthophosphate (PO_4–P), and silicate (SiO_4–Si) concentrations in the samples were measured colorimetrically. Alkalinity was determined by Gran titration, and total CO_2 (TCO_2) calculated from alkalinity and pH. The chamber volume was determined from the dilution of a known volume of an inert tracer (NaCl, NaBr or CsCl) injected at the start of each deployment. Nutrient and metabolite fluxes were calculated from the linear regression of metabolite concentration against time — typically the first 4.5 hours of each deployment.

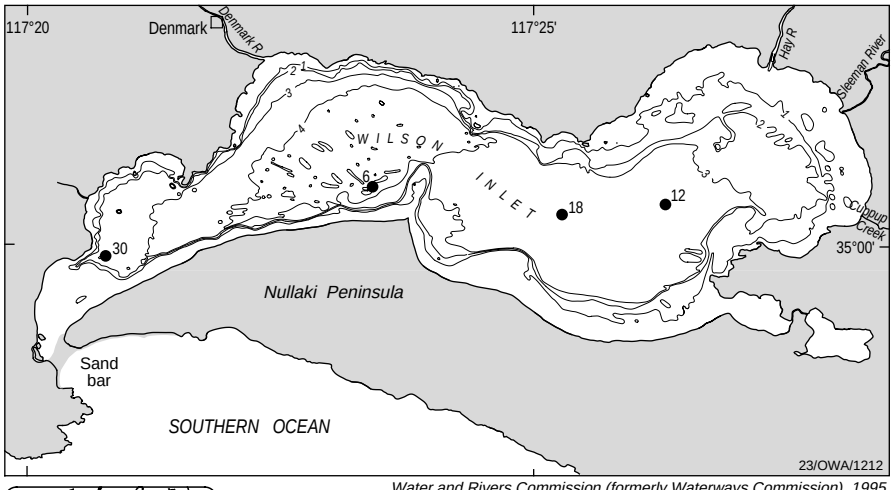

Fig. 5. Wilson Inlet study area. Bathymetric contours are annotated in metres.

Results

Winter and spring

Oxygen uptake and TCO_2 production (reflecting net respiration) were apparent in both the transparent and opaque chambers during the winter and spring surveys (Fig. 6). The similarity of the fluxes in the clear and transparent chambers indicated that no benthic photosynthesis occurred.

Summer and autumn

During the summer and autumn surveys, a net positive flux of oxygen into the water in both transparent chambers, notably in the shallower sites, contrasts with the decrease in (uptake of) oxygen and liberation of ammonia in both opaque

chambers (Fig. 7), and probably reflects MPB photosynthesis. The positive flux of oxygen in the transparent chambers was accompanied by an uptake of ammonia, presumably by the MPB.

Discussion

The seasonal variation in oxygen flux (Fig. 8) is pronounced for the transparent chambers, in which the MPB were photosynthesising during summer and autumn. In contrast, respiration in the opaque chambers showed little variation between the surveys.

TCO_2 fluxes (Fig. 8) show a similar seasonal pattern, but are ~30 per cent higher than the O_2 fluxes. The higher TCO_2 fluxes may reflect either (a) carbonate dissolution within the sediments releasing CO_2, or (b) suboxic and anoxic reduction of organic carbon (e.g., sulphate reduction) which does not consume O_2.

Nitrogen is released from the bottom mud mainly (95%) as ammonia. The ammonia, phosphate, and (high) silicate (17Si:106C) fluxes correlate well with the TCO_2 flux, suggesting that diatoms are a notable component of the labile organic carbon being consumed in the sediments (Brzezinski 1985: Journal of Phycology, 21, 347–357).

The ammonia fluxes vary between opaque and transparent chambers, but show some seasonal variation (Fig. 8). They were highest in the opaque chambers between late winter and summer, probably as a result of the increased input of organic debris to the sediments. Ammonia fluxes in the transparent chambers were similar to those measured in the opaque chambers in winter and autumn, but were near zero in summer. Little uptake of dissolved inorganic nitrogen (DIN) from the water column was measured during these seasons, despite moderately high rates of MPB photosynthesis. Assuming a typical marine composition of plankton or Redfield stoichiometry (Hillebrand & Sommer 1999: Limnology and Oceanography, 44(2), 440–446) for the MPB, we estimated that N uptake from the water column was less than 1 per cent of the potential uptake predicted from the TCO_2 flux.

The phosphate fluxes, consistently near zero, show no clear seasonal variation in either the transparent or opaque chambers (Fig. 8). The chamber data indicate that the sediments are an effective trap for PO_4–P generated within them for the prevailing conditions. Higher concentrations of PO_4–P have been recorded when the Inlet was stratified and dissolved oxygen in the bottom water was low (Water and Rivers Commission 1999: Water Resources Technical Series, WRT 14).

We provisionally estimated the annual fluxes of nutrients from sediments (Table 1) by averaging the fluxes measured in the opaque and transparent chambers and multiplying them by the area of the Inlet. The annual respiration flux of NH_4^+–N from sediments greatly exceeds the input of all forms of N from the catchment. Clearly, such a large flux of NH_4^+–N from the sediments to the water column must be balanced by a return flux, to maintain a long-term equilibrium in the system. By comparison, PO_4–P fluxes are small, but still of a similar order of magnitude to the catchment inputs.

Direct measurements of the NH_4^+–N flux show that sediments are a net source of nutrients throughout the year, despite the moderately high rates of MPB photosynthesis in summer. Whereas median rates of MPB photosynthesis in summer were 20 mmol O_2 m^{-2} day^{-1}, the median NH_4^+–N uptake from the water column was only 0.1 mmol m^{-2} day^{-1}. This is much less than the estimated requirement of 3 mmol N m^{-2} day^{-1} (calculated for a stoichiometry of 106O:16N:1P). Concentrations of DIN in the water column at the start of the summer deployments were generally low. Accordingly, the MPB apparently derived N for photosynthesis from an alternative source — perhaps the pore water just below the sediment–water interface.

The MPB clearly modified the flux of N across the sediment–water interface in summer. The role they play in controlling water quality in shallow coastal waters has been documented at only a few sites, and appears to vary. For example, water clarity and MPB productivity are highest in winter in Indian River–Rehoboth Bay, two coastal lagoons on the east coast of the US (Cerco & Seitzinger 1997: Estuaries, 20(1), 231–248). Ecosystem modelling indicated that the MPB had a major influence on nutrient cycling of nitrogen and phosphorus. In winter, when they were

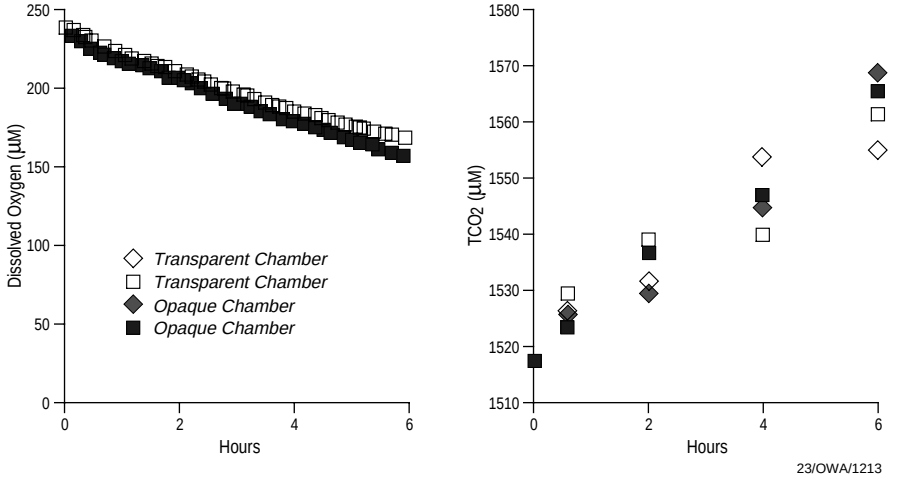

Fig. 6. Variations in dissolved O_2 and TCO_2 concentrations during a 6-hour benthic chamber deployment in November 1997. The diminishing O_2 concentration correlates with MPB respiration in each chamber, and shows no differences between the oxygen fluxes in the clear and opaque chambers.

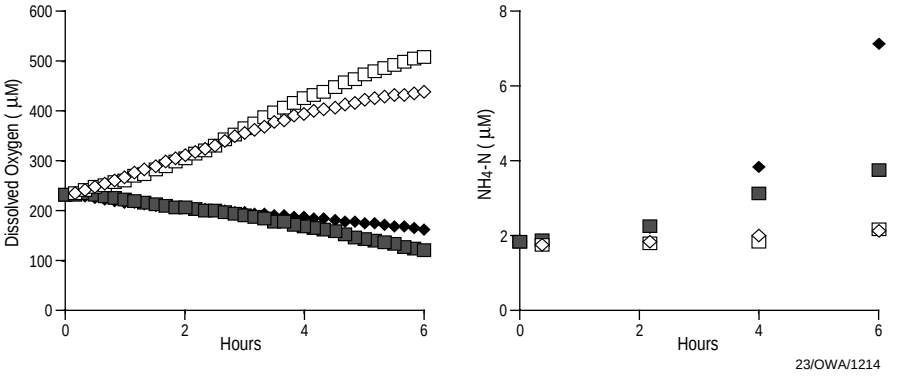

Fig. 7. Changes in dissolved O_2 and ammonia concentrations during a 6-hour benthic chamber deployment in May 1998. The increasing O_2 concentration in the transparent chambers correlates with net MPB photosynthesis.

Table 1. Nutrient fluxes for Wilson Inlet

	TCO_2	O_2	TN	DIN	NH_4^+-N	PO_4-P	SiO_4-Si
Median benthic flux (mmol m^{-2} day^{-1})	26.0	–27.5	–	1.72	1.1	0.002	4.8
Annual benthic flux (t)	–	–	–	422	267	1	2400
Catchment loads (t)	–	–	210	43	11.6	6.1	–

active and nutrients were abundant, they transferred N and P from the water column to the sediments. In summer (when they were shaded), sediment diagenesis released these nutrients to the water column, fuelling phytoplankton production. Thus the MPB provided a mechanism for maintaining high nutrient concentrations and phytoplankton production in summer. Removing the MPB from the model reduced both the sediment–water fluxes and phytoplankton production in summer.

In Wilson Inlet, water clarity and MPB activity are lowest in winter, when nutrients are entering the Inlet from the catchment. MPB primary production begins in January, after the spring phytoplankton bloom. Thus, the MPB do not provide a mechanism for the temporary storage of nutrients and release of winter nutrients. Rather, they appear to be most active at times of low nutrient concentration, and probably compete with phytoplankton and other primary producers for nutrients. The absence of MPB in this system in summer would increase the flux of nutrients to the water column and may enhance primary production by phytoplankton. Maintenance of benthic production may therefore be critical to ensuring low levels of phytoplankton and macrophyte production in summer and autumn.

Conclusions

According to benthic fluxes measured in Wilson Inlet between November 1997 and February 1999, sediments are a major source of NH_4^+–N: the annual flux of ammonia greatly exceeds the annual input of all forms of nitrogen from the catchment. In contrast, fluxes of PO_4–P from the sediments are low, and the sediments appear to be an effective trap for PO_4–P under oxic conditions.

MPB are active in summer and autumn, when the water is clear and nutrient concentrations are low. MPB primary production greatly reduced the measured NH_4^+–N flux from the sediments during these seasons, and may therefore play an important role in maintaining low levels of primary production in the water column.

Acknowledgments

The National Eutrophication Management Program, the Water and Rivers Commission (WA), and AGSO funded the study.

[1] Petroleum & Marine Division, Australian Geological Survey Organisation, GPO Box 378, Canberra, ACT 2601, Australia; tel. +61 2 6249 9434 (DJF), +61 2 6249 9589 (DTH); fax +61 2 6249 9985; email david.fredericks@agso.gov.au, david.heggie@agso.gov.au.

[2] Marine & Freshwater Resources Institute, PO Box 114, Queenscliff, Vic. 3225, Australia; tel. +61 3 5258 0224; fax +61 3 5258 0270; email a.longmore@msl.oz.au.

[3] Skyring Environmental Enterprises, 40 Atherton St, Downer, ACT 2602, Australia; tel. +61 2 6241 1036; fax +61 2 6241 9662; email see@ozemail.com.au.

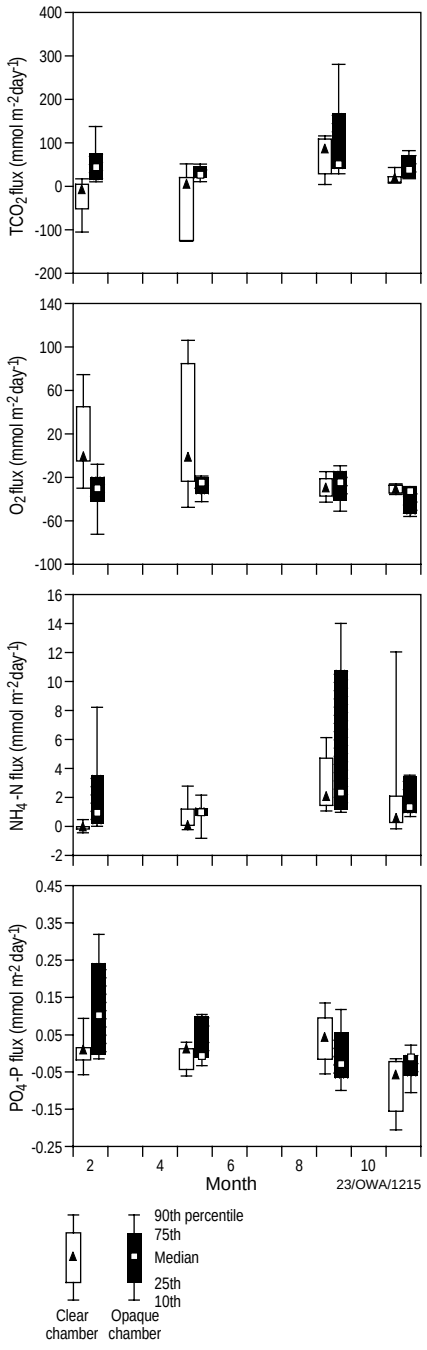

Fig. 8. Seasonal variations in metabolite fluxes from sediments.

Crustal reflectivity and bulk seismic velocity: how close is the relationship?

Alexey Goncharov[1], Peter Petkovic[1], Tanya Fomin[2], & Phil Symonds[1]

Ocean-bottom seismograph (OBS) data acquired on Australia's North West Shelf suggest that prominent seismic reflectors and changes in reflectivity patterns in conventional reflection data do not necessarily correspond to significant bulk-velocity discontinuities. If conventional reflection surveys are not supplemented by refraction/wide-angle reflection seismic studies, erroneous interpretations are inevitable.

Technological considerations

Imaging crustal reflectivity is a major aim of conventional seismic reflection technology. These images are controlled by a combination of two factors: stratification of the crust, and the spectrum of seismic signal penetrating the ground.

Crustal stratification is determined by thicknesses of layers and by contrasts in acoustic impedance (a product of density and velocity) between layers. Layers of contrasting acoustic impedance may be of different thickness, and they form various assemblages along a vertical profile through the crust.

Depending on in-phase or out-of-phase interference of reflections from individual boundaries, the total response

of any depth interval may be amplified or attenuated. Therefore, thin layers (compared to a seismic wave length, usually hundreds of metres in the lower crust) can play a prominent role in the formation of reflectivity pattern.

Importantly, bulk seismic velocity above, beneath, and even within finely stratified (in terms of acoustic impedance) depth intervals can remain unchanged, to produce a high-amplitude reflection response at near-offsets.

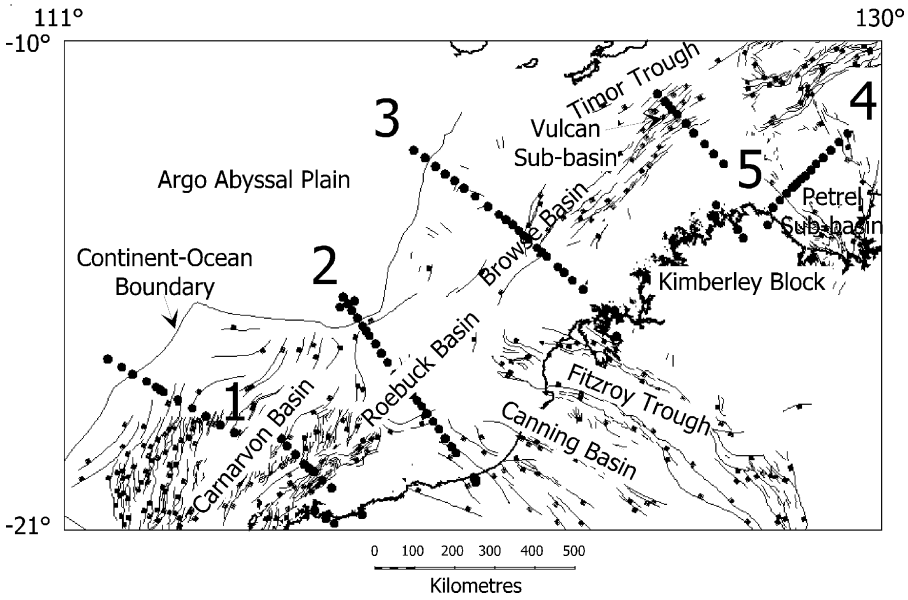

Fig. 9. Locations of the profiles in the AGSO OBS experiment, and major structural features, North West Shelf. Dots show the locations of the OBS stations. The lines are numbered: 1, Carnarvon; 2, Canning; 3, Browse; 4, Petrel; 5, Vulcan.

We have little independent information about thin density stratification of the crust, particularly in its deep part, and variations in acoustic impedance are commonly attributed to variations in seismic velocity alone. The underlying assumption for this is that there is some form of correlation between density and velocity, and, if one parameter (velocity) changes, the other parameter (density) will change proportionally.

Therefore, the effectiveness of seismic studies depends critically on how well we know seismic velocity in the ground. Modern methods of velocity analysis in conventional reflection technology predominantly make use of the curvature of the reflection travel time curve. This curvature decreases rapidly with reflection time, so that the deeper we go in the crust the less sensitive and less accurate velocity analysis becomes. Consequently, in conventional reflection technology, seismic velocities are poorly constrained in the deep part of the crust.

Conversely, refraction/wide-angle reflection seismic technology utilises observations at much larger offsets than

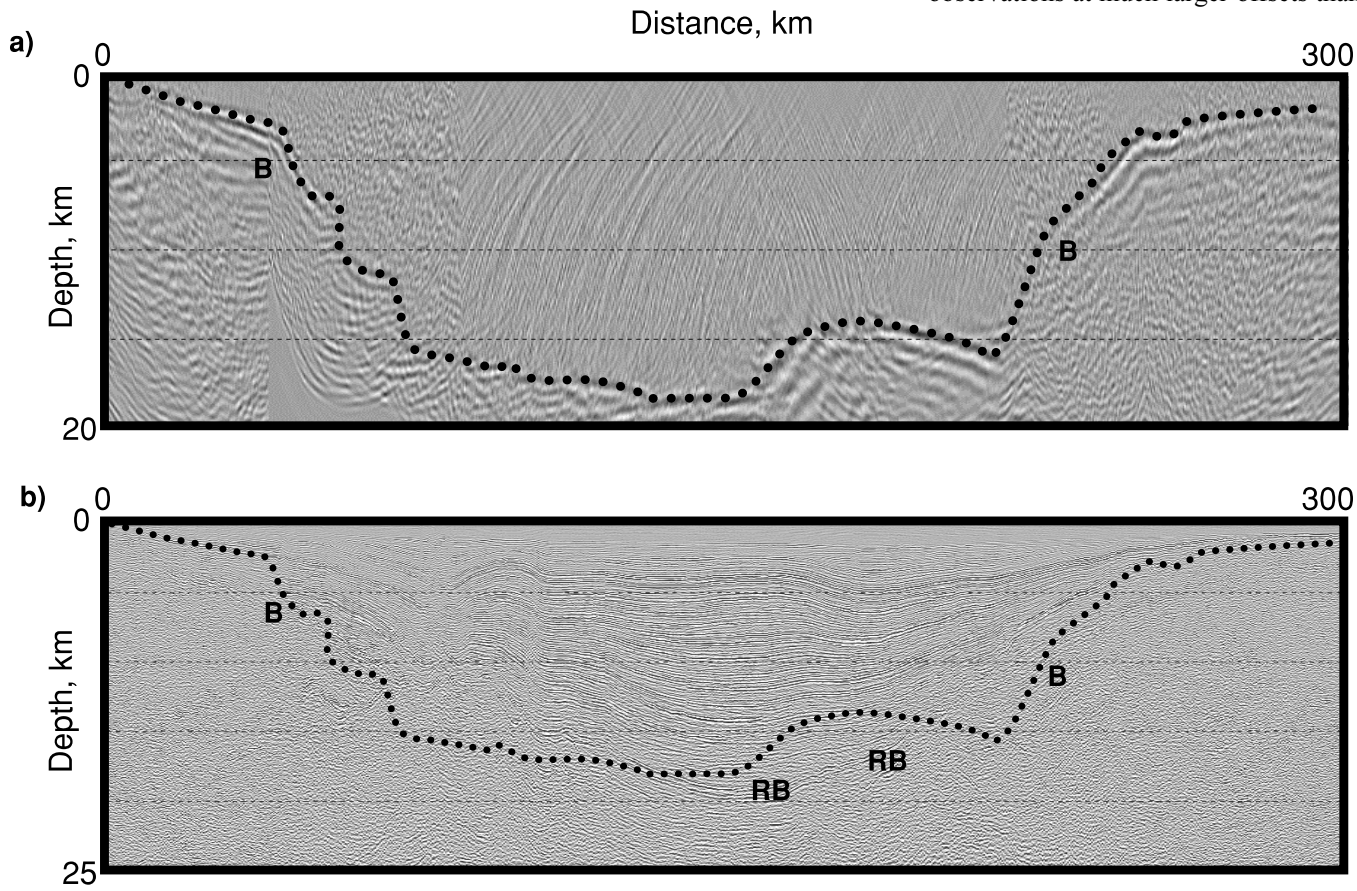

Fig. 10. (a) After-stack image of the 6.0-km/s refractor (dotted line marked B; crystalline basement?) obtained as a result of depth migration of the OBS data along the Petrel line. (b) Migrated and depth-converted conventional reflection section with the 6.0-km/s refractor superimposed on it. RB (reflection basement) index marks the bottom of continuous reflectivity in the section.

those in conventional reflection studies. As a result, it can provide much more accurate estimates of seismic velocity in the deep part of the crust.

AGSO's OBS experiment

To realise this advantage, AGSO recorded high-quality refraction and wide-angle reflection seismic data to maximum offsets of 300 km on OBSs along five profiles on Australia's North West Shelf in 1995 (cf. AUSGEO News 49, for December 1998, 8–9). All OBS transects (Fig. 9) coincided with previously acquired deep-crustal reflection profiles.

The experiment revealed that crustal reflectivity imaged by conventional reflection data does not correlate universally with crustal velocity distribution derived from the refraction/wide-angle reflection seismic data.

Petrel line

For this line, a conventional travel-time-based interpretation of the OBS data (Goncharov et al. 1998: Exploration Geophysics, 29, 384–390) was supplemented by depth migration of the recorded wave field. Our migration technique (Pylypenko 1982: in: A.S. Alekseyev, Editor, 'Application of numerical methods in studies of the lithosphere' [in Russian], Novosibirsk, Siberian Branch of the Academy of Sciences USSR, 144–154), based on both the kinematic and dynamic characteristics of the wave field recorded at large offsets, presented refraction/wide-angle seismic data in the same style as the conventional reflection data.

Such processing provided images of several refracting boundaries for the Petrel line. The 6.0-km/s refractor (B in Fig. 10) correlates poorly with the reflectivity of the crust imaged by the conventional reflection data in the centre of the line. It deviates markedly from the high-amplitude reflective band (RB), and cuts through the structure imaged by the reflection data. According to the reflectivity pattern, the RB event may represent the crystalline basement.

The 6.0-km/s refractor in the after-stack image (Fig. 10a) comprises prominent events evident in both original data and pre-stack depth-migrated images for several OBSs. The coherent stacking of several individually migrated datasets producing the image of this refractor confirms the integrity of our velocity model. Ray-tracing through this velocity model produces computed travel times which correlate well with those recorded in the experiment. Therefore, both travel-time-based interpretation and depth migration of the same dataset in this part of the section are consistent.

Consequently, the origin of the events marked RB in the conventional reflection dataset (Fig. 10b) and some other events above that level cannot be explained by changes in bulk-velocity distribution.

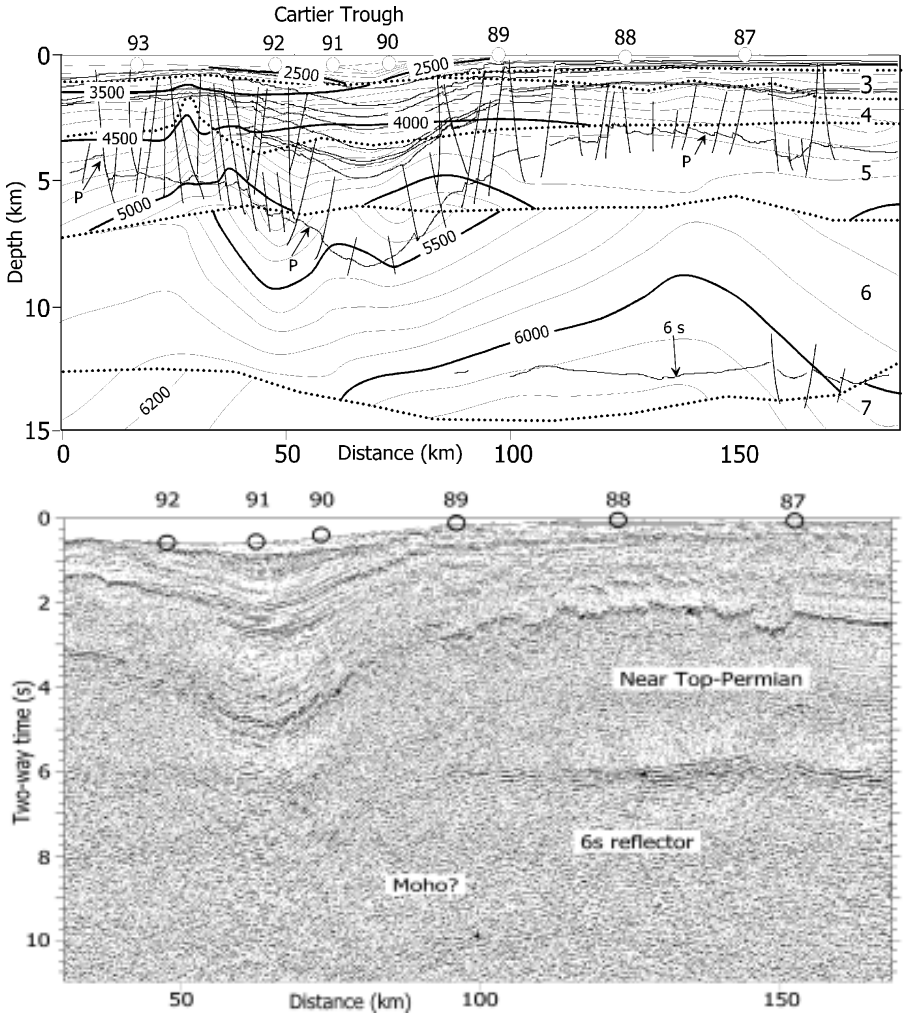

Fig. 11. (a, top) Part of the OBS-derived seismic velocity model showing isovelocity lines at 100-m/s intervals and (dotted) boundaries between layers (numbered at right). (b, bottom) Conventional reflection section along the coincident AGSO line 98/03. Circles numbered 87 to 93 are OBS locations. Thin lines in (a) are prominent horizons from the reflection section presented in (b): '6s' — high-amplitude reflector at 6 s TWT; P — near-top-Permian carbonates.

Vulcan line

The velocity model for the Vulcan line (Fig. 11a) has boundaries and isovelocity lines incongruent with the structure identified in the conventional reflection section (Fig. 11b). The top of the lower-crustal velocity-model layer 7 is near the prominent reflections at 6 s TWT, but the OBS data show no significant velocity increase (only ~200m/s) at this level. Even more incongruous, subhorizontal velocity-model layer boundaries and isovelocity lines cut across reflection boundaries beneath the Cartier Trough. Away from the trough, bulk velocity at the depth level of the near-top-Permian reflections (~2s TWT) is ~4 km/s. Closer to the centre of the trough, where the same reflections are recorded at ~5 s TWT, velocity increases to ~5.5 km/s (Fig. 11).

Prominent Moho refractions (not shown) in the wide-angle OBS data imply a velocity increase from 6.9 to 8.1 km/s. Yet the vertical reflectivity associated with the Moho is weak (Fig. 11b).

Carnarvon line

A travel-time-based interpretation of the data for this line gives a velocity model with six major layers (Fig. 12a).

Before the OBS experiment, we based a preliminary geological interpretation of the coincident reflection line primarily on the reflectivity pattern, and on the limited velocity information from expanding-spread profiles (ESP) 150–250 km southwest of the line (Mutter et al. 1989: Geology, 17, 8–15). Accordingly, we identified the upper, middle, and lower crust, the top of underplating, and the Moho

(Fig. 12c). The upper crust, apparently block-faulted, has subparallel to parallel reflectors showing mainly horizontal layering. The middle crust is characterised by discontinuous, undulatory, high-amplitude reflectors. The lower crust is transparent. Underplating was deduced from reflectivity pattern, not from velocity estimates. The top of the underplated layer was taken to coincide with a band of low-frequency, very high-amplitude reflectors 13–17 km deep (one of the most prominent features in Fig. 12c). From the ESP results, we estimated the P-wave velocity below these prominent reflectors to be ≥7 km/s. High-amplitude discontinuous events or a weak band of reflectors ~14 km deep, primarily in the northwest part of the line (beneath oceanic crust), represent the Moho.

This interpretation shows some conformity with the new OBS-derived velocity model — for example, the interpreted base of the middle crust is close to the boundary between layers with velocities of 4.3–5.0 and 5.7–6.4 km/s (Fig. 12a, b). Even so, some remarkable incongruities between the interpretation and the velocity model are apparent (Fig. 12b, c).

Firstly, the prominent reflectivity 13–17 km deep in the conventional reflection data does not correspond to any significant velocity increase imaged by refraction/wide-angle techniques. The velocity below that level estimated from the OBS data is in the range 5.7–6.4 km/s, considerably lower than that indicated by the ESP data.

Secondly, the local velocity increase in the lens-shaped lower crustal body 15–23 km deep (Fig. 12a) produces no noticeable response in the conventional reflection section (Fig. 12b, c).

Finally, the Moho occurs at an average depth of ~18 km, in contrast to 14 km in the preliminary interpretation. This implies a considerably thicker oceanic crust beneath the Gascoyne Abyssal Plain in the outer part of the Carnarvon transect.

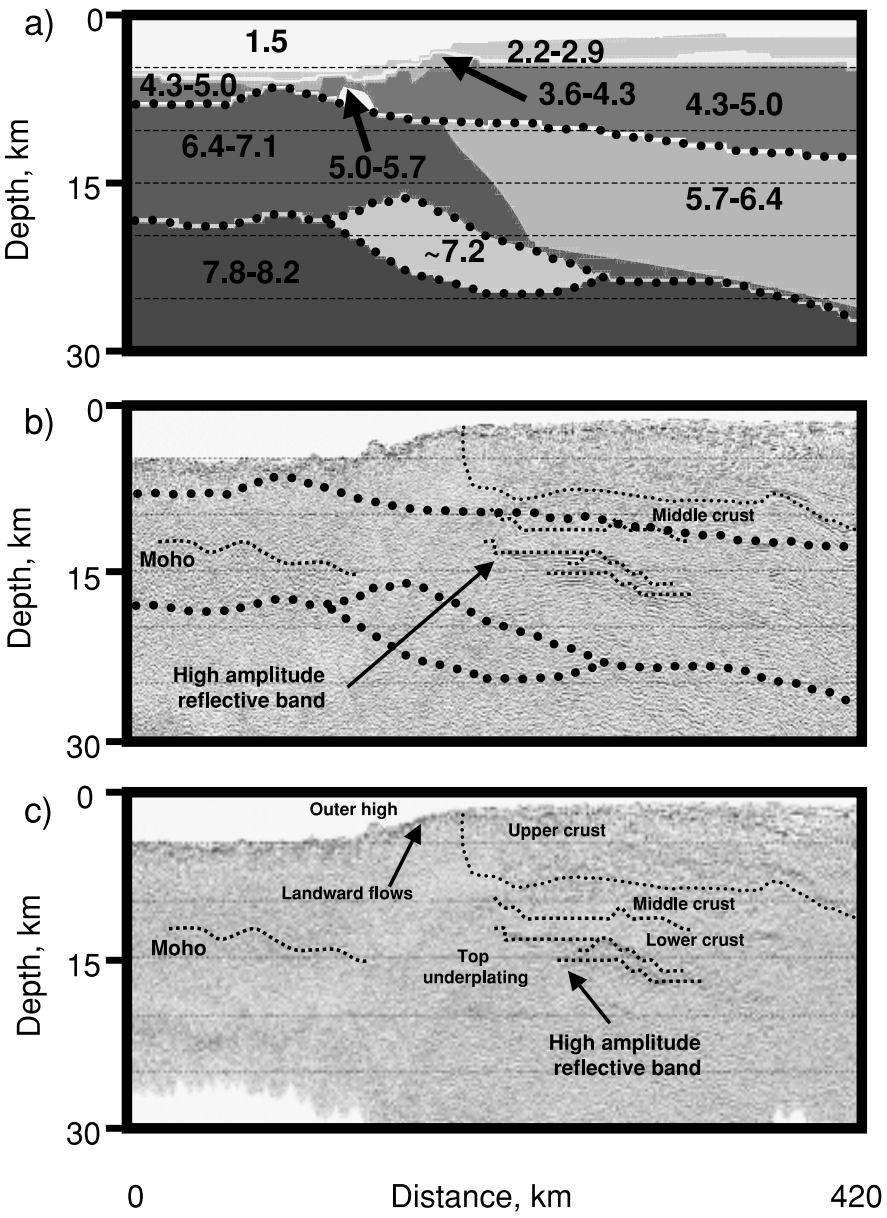

Fig. 12. (a) Seismic velocity model for the Carnarvon line from the OBS data. (b) and (c) Reflection section along the coincident reflection line depth-converted with OBS-derived velocities (b), and with CDP-derived velocities (c). Large dots in (a) mark some velocity boundaries discussed in the text, and small dots in (c) show some elements of interpretation discussed in the text. Both sets of dots superimposed on top of the reflection section in (b).

Consequences for the petrological interpretation

Inaccurate velocity estimates will lead to unrealistic estimates of the petrology of rocks at depth. The Carnarvon line example can be used to quantify this observation.

In our preliminary geological interpretation, we correlated the top of underplating in the Carnarvon line (Fig. 12c) with the top of a mafic layer intruded into the lower crust as a result of partial upper-mantle melting. We can test the validity of this correlation by using the petrophysical modelling technique of Sobolev & Babeyko (1994: Surveys in Geophysics, 15, 515–544; Goncharov et al. 1997: AGSO Research Newsletter 26, 13–16) to interpret the OBS-derived velocity model in terms of bulk rock geochemistry.

A comparison of the representative velocity–depth function in the southeast part of the Carnarvon line (Fig. 13b) with the results of petrophysical modelling (Fig. 13a) shows that velocities 5.7–6.4 km/s in the lower crust cannot correspond to mafic rocks, even under high heat-flow conditions. Though a rock will record its lowest possible velocity under a high-temperature regime, our modelling (even assuming such conditions) shows that velocities 5.7–6.4 km/s are restricted to rocks with granite-type bulk compositions (Fig. 13a). Mafic rocks (gabbro-type bulk composition) have velocities mainly in the range 7.1–7.8 km/s (Fig. 13a). The velocities of rocks with low-garnet–high-plagioclase gabbroic compositions in the lower crust rarely approach 6.4–7.1 km/s. Therefore, even the layer with velocities of 6.4–7.1 km/s in the northwest part of the Carnarvon line (Figs. 12a and 13b) is

unlikely to represent purely mafic rock. Rather, these velocities correspond mainly to granite-to-diorite-type bulk compositions and their mixtures (Fig. 13a).

Our preliminary interpretation, therefore, does not satisfy the velocity information derived from the OBS experiment in the northern Carnarvon Basin. Even so, the lens-shaped body distinguished by the OBS data in the lower crust (Fig. 12a) has a velocity (~7.2 km/s) consistent with a gabbroic composition (Fig. 13a). Therefore, underplating may be a feature of the northern Carnarvon Basin — but ~90 km farther northwest and ~5 km deeper than we originally interpreted.

Speculations on the origin of discrepancies between reflectivity and bulk-velocity changes

According to Berzon (1976: 'Seismic prospecting in finely stratified media' [in Russian], Nauka Press, Moscow), simple sharp boundaries with step-like velocity increases produce prominent seismic responses at large offsets. The same applies to transitional layers whose velocities gradually increase with depth. Near-vertical reflections in both cases may be 10–100 times weaker than the wide-angle ones. Conversely, assemblages of thin (on a seismic-wave-length scale) layers with sharp velocity contrasts at their boundaries are more likely to produce high-amplitude near-vertical reflections and only weak responses at large offsets.

Accordingly, we suggest that the high-amplitude reflective band 13–17-km deep along the Carnarvon line (Fig. 12b) represents thin interlayering of high- and low-velocity material (e.g., sheet intrusives; mylonites associated with fault zones; etc.). Despite considerable velocity contrasts at the boundaries of individual thin layers within this depth interval, bulk velocities above and below this layer are similar. Otherwise, a prominent response at large offsets would have been expected in our dataset.

The same thin layering mechanism may explain the origins of the reflectivity at ~15–20-km depth along the Petrel line (Fig. 10b), and the 6-s reflector on the Vulcan line (Fig. 11b).

Why the finely stratified assemblages do not coincide with boundaries where bulk-velocity changes significantly (e.g., the 6.0-km/s refactor along the Petrel line) remains unclear. It is also not clear why the Moho in the Carnarvon and Vulcan sections is more likely to be a sharp and simple velocity boundary or a transitional layer rather than a finely stratified interval; a marked velocity contrast at this boundary coincides with only weak near-vertical reflections.

Beneath the Cartier Trough, where isovelocity lines are incompatible with the structure imaged by the conventional reflection data (Fig. 11), the progressive velocity increase with depth can probably be attributed to compaction due to increasing geostatic pressure. This smooth trend would be superimposed on the original fine stratification, which in turn probably would control the reflectivity pattern, whereas bulk-velocity changes would be determined by compaction-related factors.

In summary, reflective boundaries and bulk-velocity boundaries in the crust are commonly controlled by different factors whose causes require further research. Whereas conventional reflection technology tends to highlight fine seismic stratification of the crust, refraction/wide-angle reflection technology images better bulk-velocity changes in the crust. Only a combination of both techniques offers clues to a consistent geological interpretation of seismic data.

Acknowledgments

We thank John Kennard and Ken Muirhead for reviewing a prior draft, and Clive Collins for fruitful discussions.

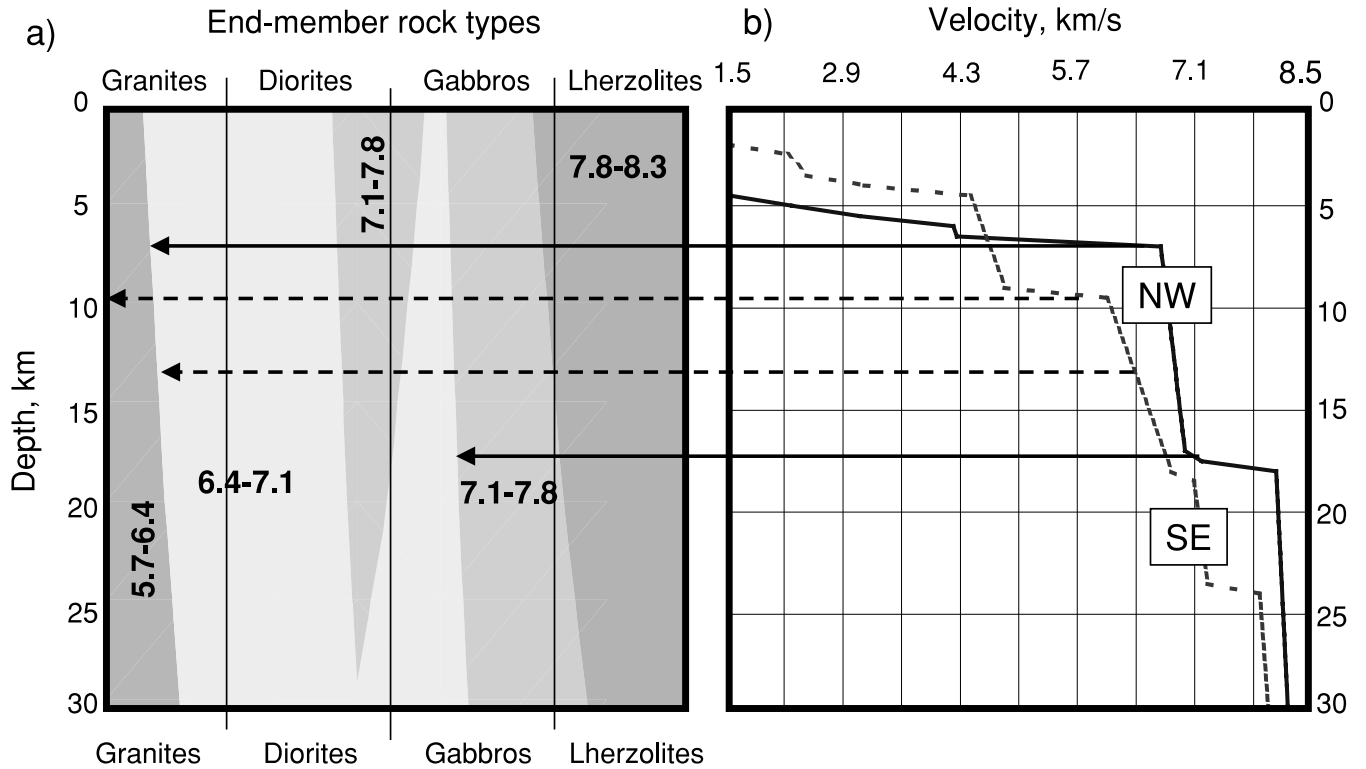

Fig. 13. (a) P-wave velocity in various rock types as function of depth computed for high heat flow, and (b) representative 1-D velocity models in the northwest and southeast parts of the Carnarvon line. The bulk geochemical composition within each rock type is constant, and the mineralogical compositions are allowed to vary to account for equilibration at the pressures and temperatures likely to have existed when the rock was formed.

[1] Petroleum & Marine Division, Australian Geological Survey Organisation, GPO Box 378, Canberra, ACT 2601; tel. +61 2 6249 9595 (AG), +61 2 6249 9278 (PP); fax +61 6 249 9980; e-mail alexey.goncharov@agso.gov.au, peter.petkovic@agso.gov.au.

[2] Minerals Division, Australian Geological Survey Organisation, GPO Box 378, Canberra, ACT 2601; tel. +61 2 6249 9725; fax +61 6 249 9972; e-mail tanya.fomin@agso.gov.au.

Ocean-floor volcanism in the Lachlan Fold Belt: new evidence from the Wyalong area, New South Wales

Morrie Duggan[1] & Patrick Lyons[2]

Geochemical data indicate that a recently recognised sequence of Ordovician volcanic rocks (the Narragudgil Volcanics) south of Wyalong (NSW) accumulated in an oceanic environment, either in a mid-ocean ridge (MORB) or back-arc basin (BAB) setting. These volcanics occur in the same package of highly magnetic rocks with a complex magnetic signature as the Gidginbung Volcanics, host to the Temora gold deposit. They were previously considered to be part of the Gidginbung Volcanics, although Warren et al. (1995: Cootamundra 1:250 000 Sheet Explanatory Notes, Geological Survey of New South Wales) noted the presence of rocks in this area as having "…affinities to the older Jindalee Group with which they may be correlatable".

The Narragudgil Volcanics are sparsely exposed in a few localities within the Gilmore Fault Zone (Gilmore Suture) immediately south and east of the township of Wyalong (Fig. 14). In Millers Quarry, they consist of basalt characterised by a penetrative (at outcrop scale) subvertical fabric, in the form of anastomosing planes of high strain

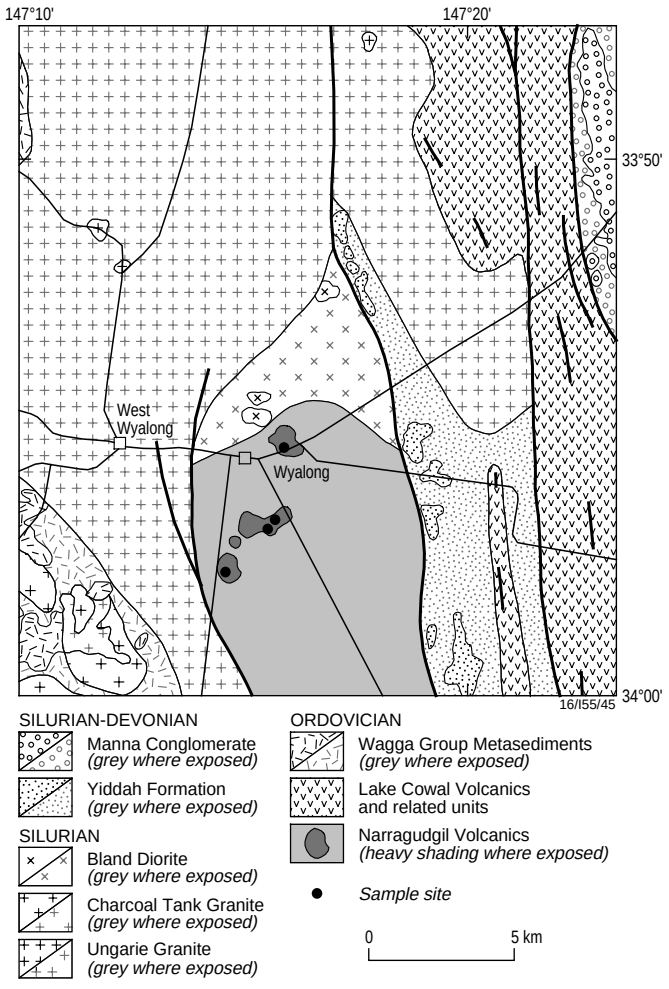

Fig. 14. Geological sketch map of the West Wyalong area showing the exposed extent (heavy shading) and interpreted distribution (light shading) of the Narragudgil Volcanics and other rock units.

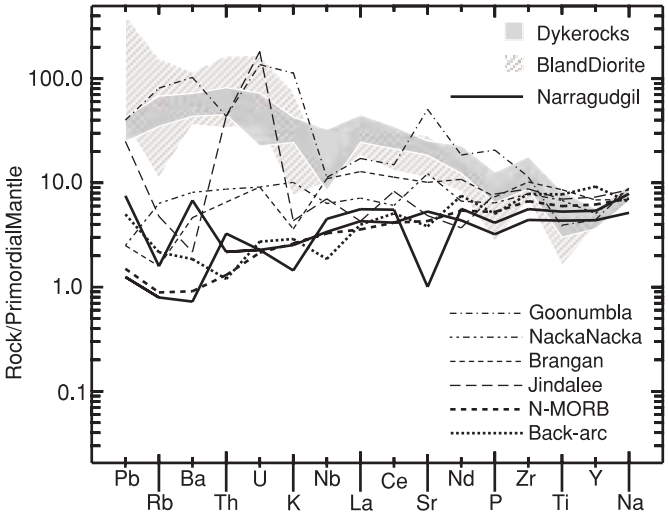

Fig. 15. Primordial mantle-normalised multielement abundance diagram (spidergram) for basalts of the Narragudgil Volcanics and other rocks. Data sources: Narragudgil Volcanics, Bland Diorite, and dyke rocks (this study); Goonumbla Volcanics (Clarke 1990: op. cit.); Nacka Nacka Volcanics (Wyborn 1996: 'Geology, chemistry and gold/copper potential of the Temora belt and adjacent Gilmore Fault System', AMIRA Project P425, Report; Brangan Volcanics (D. Wallace, personal communication); Jindalee Group (Warren 1995: op. cit.); N-MORB (Sun & McDonough 1988: in Saunders & Norry (editors), 'Magmatism in the ocean basins', Journal of the Geological Society of London, Special Publication 42, 313–345; BAB (Pearce et al. 1995: in Smellie (editor), 'Volcanism associated with extension at consuming plate margins', Geological Society, Special Publication 80, 53–75.

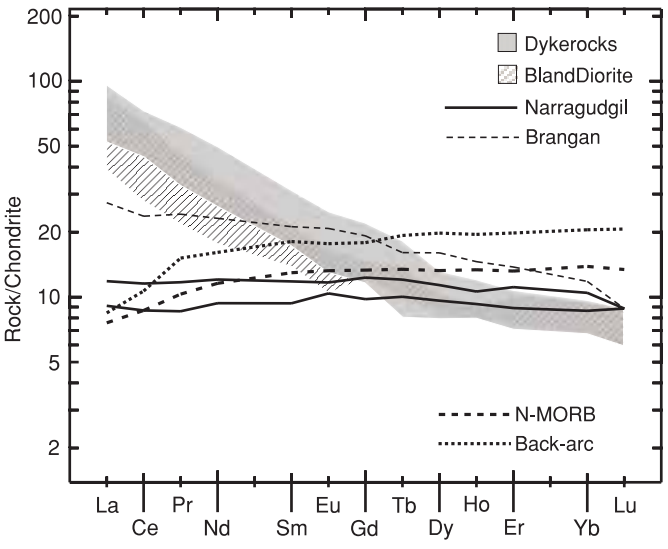

Fig. 16. Chondrite-normalised rare-earth-element abundance diagram for basalts of the Narragudgil Volcanics and other rocks. Data sources as for Fig. 15.

up to a few centimetres wide, produced during shearing or faulting. Because the strain was partitioned, these planes separate sheets of massive, essentially undeformed metabasalt, typically 20–40 cm across, which have the superficial appearance of sheeted dykes. This impression is further enhanced by the presence of a swarm of intermediate dykes, typically 1–3 m across, subparallel to the dominant fabric. The dykes, which lack the structural fabric of the basalts and clearly postdate the deformation, have a distribution and geochemistry in common with the Lower Silurian Bland Diorite.

The Narragudgil Volcanics are geochemically primitive [$100Mg/(Mg+Fe^{2+}) = 56–64$] olivine tholeiites with low K_2O (<0.2 wt %) and K/Na ratios. Their trace-element contents — characteristically depleted in large-ion lithophile element (LILE) abundances (Fig. 15) and having a flat rare-earth-element distribution (Fig. 16) — are typical of ocean-floor basalts erupted in either a MORB or BAB setting. Some scatter in the trace-element data probably reflects element mobility during metamorphism. However, the overall character of the elemental abundances is consistent, and cannot be an artefact of the metamorphism. In addition, two other samples not plotted on Figures 15 and 16 — an altered dolerite and a fine-grained quartz-rich amphibolite with major-element abundances reflecting basalt weathered before metamorphism — show the same broad trace-element distributions, albeit with rather more scatter in some elements.

The geochemical characteristics of the Narragudgil samples contrast markedly with the associated dyke suite and the Bland Diorite, which show higher K_2O (up to 2.5 wt %) and more enriched LILE and light rare-earth-element abundances. In these aspects, the Narragudgil Volcanics also contrast markedly with the well-documented high K_20 and K/Na ratios and strong LILE-enrichment exhibited by the Ordovician Goonumbla Volcanic Group and related units of the eastern Lachlan Fold Belt — including the Nash Hill, Parkes, Wombin, and Lake Cowal Volcanics (e.g., Clarke 1990: in Clarke & Sherwin (Editors), Records of the Geological Survey of New South Wales, 23, 97–136). The Narragudgil unit otherwise shares similar geochemical characteristics, including depletion in K and LILE, with other units in the eastern Lachlan Fold Belt — namely, the Brangan Volcanics in the Grenfell area (D. Wallace, AGSO, personal communication), the Nacka Nacka Volcanics in the Tumut area, and basalt from the Jindalee Group (Fig. 15). Note that the high U, Th, and Pb shown by the Jindalee sample appear to be anomalous, and probably reflect the age and lack of precision of the analysis. The Narragudgil Volcanics evince a slight relative depletion in high-field-strength elements compared with these other units and with typical MORB and BAB compositions. Even so, the abundances in all samples fall within the range encountered in typical mid-ocean ridge and back arc settings.

It is not clear if the Gilmore Fault Zone is a terrane boundary (e.g., Stuart-Smith 1991: BMR Journal of Australian Geology & Geophysics, 12, 35–50). However, the presence of ocean-floor basalts within it opens up the possibility that the Narragudgil Volcanics represent a sliver of sea-floor obducted onto the volcanic arc during closure of the Wagga Marginal Basin in the Middle to Late Ordovician.

The ocean-floor affinity of the Narragudgil Volcanics suggests that they are unlikely to host any porphyry-related Cu–Au systems. However, they may be prospective for Cyprus-type copper deposits.

[1] Formerly Minerals Division, Australian Geological Survey Organisation; now 14 Bird Place, Flynn, ACT 2615; tel. +61 2 6258 8032; email morris@guarana.org.

[2] Minerals Division, Australian Geological Survey Organisation, GPO Box 378, Canberra, ACT 2601; tel. +61 2 6249 9763; fax +61 2 6249 9983; email patrick.lyons @agso.gov.au.

The evolution of geoscientific metadata

Roderick J. Ryburn[1]

The fruits of geoscientists' labours are consigned increasingy to computer files. Although the capacities of electronic media are expanding rapidly, the means of keeping track of all these files is lagging. Knowledge-based organisations like AGSO need the electronic equivalent of libraries to house this information, the analogue of library catalogues to allow us to find critical bits, and the equivalent of librarians to manage the metadata. Files worth keeping must be kept permanently online, referenced by a metadatabase, accessible from the Web, and compliant with changing hardware, software, and data standards.

The way it was

Back in the 'paper epoch' — just 20 years ago, but extending all the way back to the Great Library at Alexandria — scientists strove to record the fruits of their work in papers, diagrams, maps, and books. Apart from verbal reports (lectures, demonstrations, sound and visual recordings, etc), most scientists chose to record their endeavours as paper-based products. It was truly a case of publish or perish! Geoscientists did not differ in this regard, though they tended to produce more maps than most other scientists.

The final resting place for all these paper products was unquestionably a library. Libraries offered the most enduring facility for preserving the scientists' published works and making them accessible to others for the foreseeable future.

As libraries evolved, so too did the means of locating items in their ever-growing collections. Catalogues appeared as the first metadata system for libraries, and later evolved into the card-index systems that most of us still remember. Library catalogues evolved to such an extent that whole university departments were set up to train librarians in the complex subject of library cataloguing. Their evolution continued through the advent of microfilms and microfiche, but it is the rise of computer communications, and the World Wide Web in particular, that has dramatically changed the way we must now think about library catalogues.

The way it is

For the last 20 years, the electronic medium has accounted for the dissemination of an ever-increasing share of scientists' primary outputs. Geoscientists, perhaps to a degree greater than many other scientists, have to contend with a large variety of electronic outputs — mostly in the form of digital computer files. These now include files from wordprocessors, spreadsheets, databases, email, the Web, image and seismic processing, airborne geophysics, radar, marine surveys, laboratory instruments, GIS, CAD, and specialised 3D mining and petroleum packages.

Some digital geoscientific information now finds its way into corporate databases, which should come with in-built metadata. However, such highly structured data systems will never completely eliminate the need to store less structured static information in files of various sorts. The traditional scientific paper or report will remain a valid output for the foreseeable future, and there will always be a need to represent information that is too specialised to fit into a standardised database system. Although static files may soon be stored in a database management system, rather than in a traditional computer filing system, this does not negate the need for adequate metadata.

The current tendency is to group computer files produced by a project onto a CD–ROM (soon to be overtaken by the DVD, the digital versatile disc). In this form, the information can be stored and catalogued in libraries, as for paper publications. Unlike paper publications, though, there is no guarantee that such CDs will be easily

readable in 10 years time, let alone 100 years on. The problem is not so much the longevity of the medium (although this could also be a problem) as the rapidity with which hardware, software, and data structures are currently evolving. Files written by specialised software, such as GIS systems and 3D mining packages, often change their format with software upgrades. Five years on, finding a previous version of a program may be a nuisance. Ten years on it may be virtually impossible, particularly if the operating system has also changed. So, placing files on a CD, or even a DVD, is not the long-term solution it first appears.

The problems we are currently facing are to do with the transition between the old paper-based systems and the new online methods that have yet to become fully established. Libraries are trying to come to grips with the storage of, and access to, digital outputs, but still have some distance to travel before they can claim success. Conventional corporate network systems and disc directories lack the necessary metadata facilities, and files can all too easily be lost in an ephemeral maze of hierarchical computer directories. Right now, there is a significant danger that we may lose much of our current geoscientific output. We need to upgrade our facilities and techniques for handling metadata.

The way it will be

The ultimate solution to the problems outlined above is to ensure that all computer files worth keeping are stored online in conjunction with a corporate metadata system. The metadata system should not only describe the format and contents of the files but also include pointers to enable the automatic retrieval of files. In storage systems other than small ones, if the metadata do not exist, the file cannot be found, so it might as well not exist. The supply of adequate metadata thus becomes an absolute necessity. The files need not be instantly accessible, but they can reside in automated data warehouses, such as tape 'silos'. Computer object-reference systems — like Open Systems' CORBA (Common Object Request Broker) and Microsoft's DCOM — are now showing the way that digital information can be accessed over the corporate network without the need to know file locations on network discs or tape silo systems. A spin-off is that all information becomes potentially accessible via the Web and thus much more e-commerce friendly.

Only in this way can we be sure that the problem of evolving file formats is easily tackled, and that all information can be kept up to date with respect to current file types, formats, data standards, software, and operating systems. When all files of a certain type and vintage can be automatically identified and located, then it becomes a relatively trivial exercise to extract these files, translate them into the required new format, and replace them in the 'warehouse'. The process can be largely automated, and all information thus kept safe and in currently readable forms. Right now, digital information can routinely be kept more safely than paper information in libraries. With good metadata facilities, we can ensure that the same information becomes immune to the rapid evolution of software, particularly specialised software. The key is good metadata.

Metadata on the web

Mention metadata in connection with the worldwide web — and most people immediately think of search engines, like Yahoo and AltaVista. Wonderful as they are, these search engines are text-based and somewhat hit-and-miss when compared with a properly structured metadata system, such as a library catalogue. Although web access is now virtually mandatory for any comprehensive metadata system, the metadatabase should reside in a corporate-strength relational database management system. This can now be done fairly easily by providing an attractive web interface (or interfaces) to the corporate metadatabase. Metadata standards and interchange protocols, such as the 'Dublin core' metadata standard and the 'Z39.50' protocol for the interoperability of library catalogues, will eventually lead to transparent access to metadata, irrespective of location or custodianship. Similarly, the Australian Spatial Data Infrastructure (ASDI) initiative envisages distributed custodianship of spatial databases, with nodes or 'clearing houses' from which the users can query standard metadata in the distributed databases and obtain just the spatial information they require.

The 'AGSO catalog'

In the absence of an off-the-shelf system spanning the full breadth of digital geoscientific information, AGSO has opted to establish its own minimalist system, called the 'AGSO catalog' (Ryburn 1999: *in* AGSO Record 99/24), which is designed to capture metadata on hardcopy output and computer files alike. In addition to providing the outside world with a window into AGSO's outputs, the 'catalog' satisfies our internal requirements for a comprehensive geoscientific metadata system, while tracking the progress and quality of all outputs. A text-based web interface for the products in the 'catalog' can be seen at *http://www.agso.gov.au/databases/catalog/agsocat.html*, but this will soon be joined by a spatially based web interface. Developed from AGSO's former 'Products database', with information on all products sold by the AGSO Sales Centre, the 'catalog' includes metadata on datasets, 'resources', external articles, and products. It also draws on a much wider community of contributors for additions to its information base. The 'catalog' is seen as the key to future systems of online access to, and distribution and sales of, AGSO's information.

In addition to the 'catalog', AGSO's spatial outputs — e.g., maps, images, and GIS datasets — are in the 'GEOMET' spatial metadatabase, which is on AGSO's web site at *http://www.agso.gov.au/information/structure/isd/database/metadata.html*. This metadatabase closely follows the ANZLIC (Australia New Zealand Land Information Council) guidelines for the transfer of metatadata. However, it is generally unsuited to AGSO's non-spatial outputs, and the entry of metadata is too tedious and specialised for general use. The dilemma we face in AGSO is that many of our products bridge the gap between the text-based library world, represented by the 'Dublin core' metadata standard, and the spatial dataset world represented by the ANZLIC guidelines. The 'AGSO catalog' and 'GEOMET' systems go some way towards satisfying both these requirements. Only by making sure that our metadata remain current and well organised in relational databases can we be confident of keeping up with further convergence and evolution in metadata standards.

Conclusions

- Traditional, paper-based methods of handling information are disappearing.
- Geoscientists now produce an enormous range of data and computer-file types.
- Storing away computer files on CDs or DVDs is not a long-term solution.
- Files worth keeping must be stored online or, at least, in an 'active archive'.
- Metadatabases that refer to online files are fast becoming an absolute necessity.
- Corporate metadatabases must have the means to automatically access online files.
- Files must be kept up to date with respect to evolving data standards and software.
- Large organisations must employ professionally qualified metadata custodians.
- Librarians are the traditional metadata experts, but they should expand their roles.
- Corporate metadata must be stored in a relational database with web interfaces.
- The 'AGSO catalog' and 'GEOMET' spatial metadatabases are a good start for AGSO.

[1] Information Management Branch, Australian Geological Survey Organisation, GPO Box 378, Canberra City ACT 2601; tel. +61 2 6249 9605; fax +61 2 6249 9984; email rod.ryburn@agso.gov.au.

Scientific visualisation and 3D modelling applications for mineral exploration and environmental management

John Wilford[1]

Introduction

Complex spatial information for geological, geomorphological, and geophysical studies is generally stored in relational databases and displayed as either discrete (point, line, or polygon) or raster (e.g., satellite and airborne images) datasets. For their analysis and integration, these datasets depend mostly on commercial GIS software operating largely in 2D space — a severe restriction for Earth-science datasets in 3D, or 4D if time is included. Most subsurface information is interpreted and displayed thematically in 2D (e.g., depths-to-basement contour maps, magnetic/bedrock polygons, cross-sections, fence diagrams, drill profiles, and block sections). Subsurface variation and composition is typically poorly depicted on most geological and regolith maps.

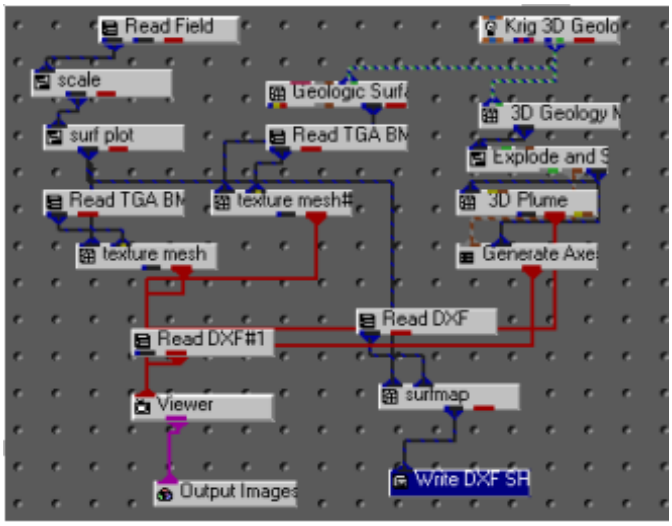

Fig. 17. Data-flow processing network.

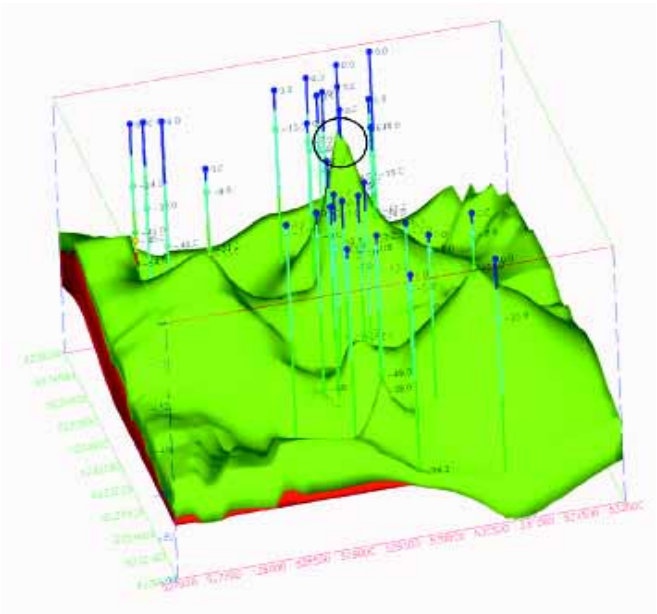

Fig. 18. A 3D regolith block model constructed from drillholes. Vertical pipes mark the position of the drillholes. Inconsistent logging of the drillcore can result in anomalous spikes in the isosurfaces (3D surface of equal value) as indicated by the circle.

Recent advances in GISs and in visualisation hardware and software have fabricated an interactive environment for the desk-top operator to display, analyse, and integrate geoscientific information in a 3D context. AGSO scientists are keeping abreast of these advances, and using computer-generated 3D models and visualisation techniques in several projects to help analyse, interpret, and communicate information for mineral and petroleum exploration and environmental management.

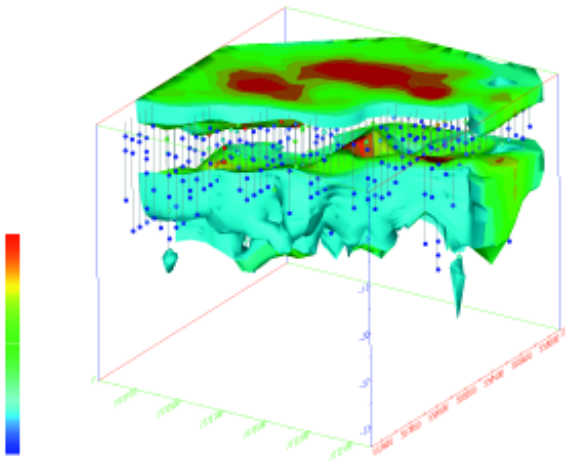

Fig. 19. A 3D regolith model based on drillhole data from the Tanami area. Gold concentrations are combined with the regolith units to better resolve the relationships between the regolith and supergene gold dispersion. Colours from blue to red indicate increasing gold concentration. Drillholes are shown as pipes; geochemical samples, as dots.

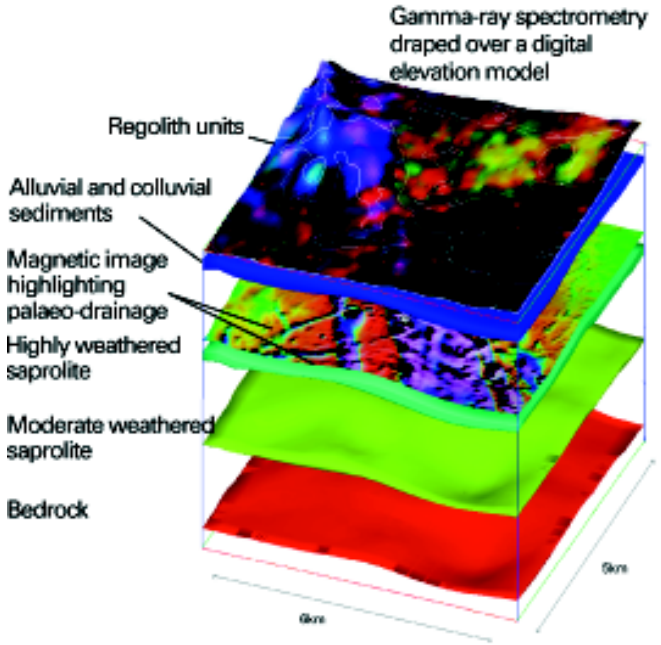

Fig. 20 A 3D block model displaying surface topography (DEM) and airborne gamma-ray spectrometry over regolith units in part of the Gilmore area. A magnetic image highlighting palaeochannels is floated between the transported and *in situ* contact.

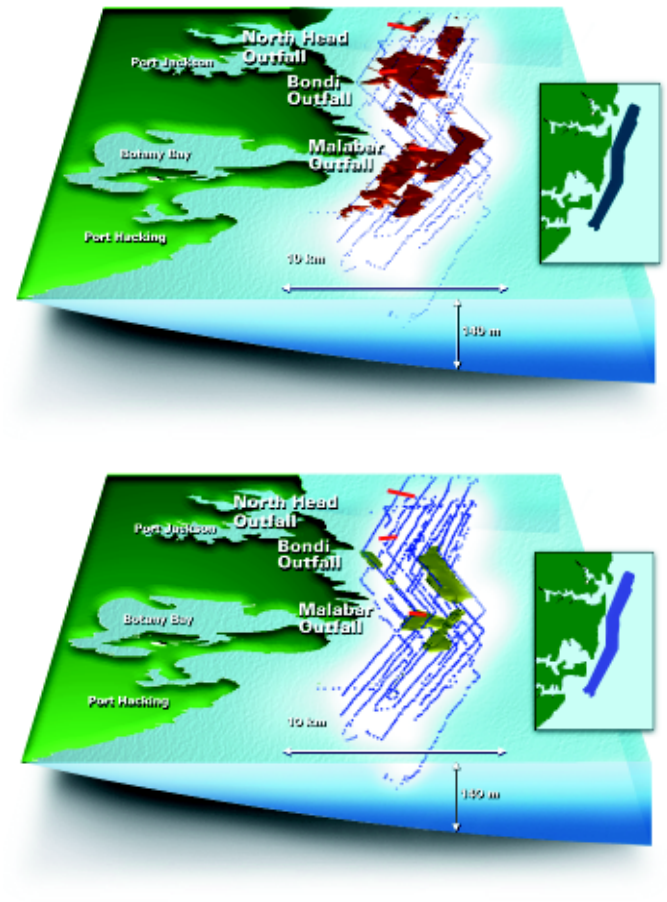

Fig. 21. Geochemical modelling of environmental oceanography data. (a, top) A 3D propane geochemical plume off Sydney. The plume has been clipped to show values greater than .25 ppm. (b, bottom) A 3D methane plume clipped to values above 12 ppm. The land is shown in green. Dots correspond to geochemical samples; red rectangles, ocean outfall sites.

3D visualisation

Scientific visualisation uses computer-generated imagery to facilitate an interpretation or investigation of scientific phenomena. For geoscientific applications, computer-graphic-visualisation tools provide an interactive environment whereby information from different sources is integrated and modelled in 3D. A range of 3D visualisation software packages is available; each has different levels of functionality, sophistication, and compatibility with commonly used 2D GIS platforms (e.g., ArcView, Arc/Info, and MapInfo).

Data processing

Data processing in visualisation and modelling software can be broadly divided into either data-flow or non-data-flow systems. Data-flow systems consist of modules that perform specific functions. These modules are linked together in a data processing pathway from the unprocessed datasets to the final enhanced display. Non-data-flow systems are more traditional in their architecture, and have either command-line or menu-driven operations.

The figures presented herein were generated from the data-flow 'Environmental visualisation system' (EVS), in which the user constructs a processing network of icons (selected from stored libraries) for performing the range of operations (e.g., gridding, filtering, subsampling). Networks provide an excellent pictorial representation (Fig. 17) of the data processing pathway, and enable the user to customise for specific applications. Once a network has generated a 3D object, various tools are available to rotate, shift, colour, resize, and illuminate it.

3D models and data uncertainty

Surface datasets are moderately easy to collect and analyse — viz., digital elevation models (DEMs), airphotos, and Landsat Thematic Mapper (TM) and gamma-ray spectrometric imagery, which provide continuous topographic, compositional, and geochemical information.

In contrast, subsurface information is generally localised (e.g., mines and borefields). It is generally restricted to points or profiles down a drillhole or to vertical slices (e.g., seismic profiles) and modelled imaged surfaces (e.g., depths to magnetic basement, or electromagnetic (EM) depth to weathered basement). For 3D subsurface volumetric models derived from drillhole datasets, statistical

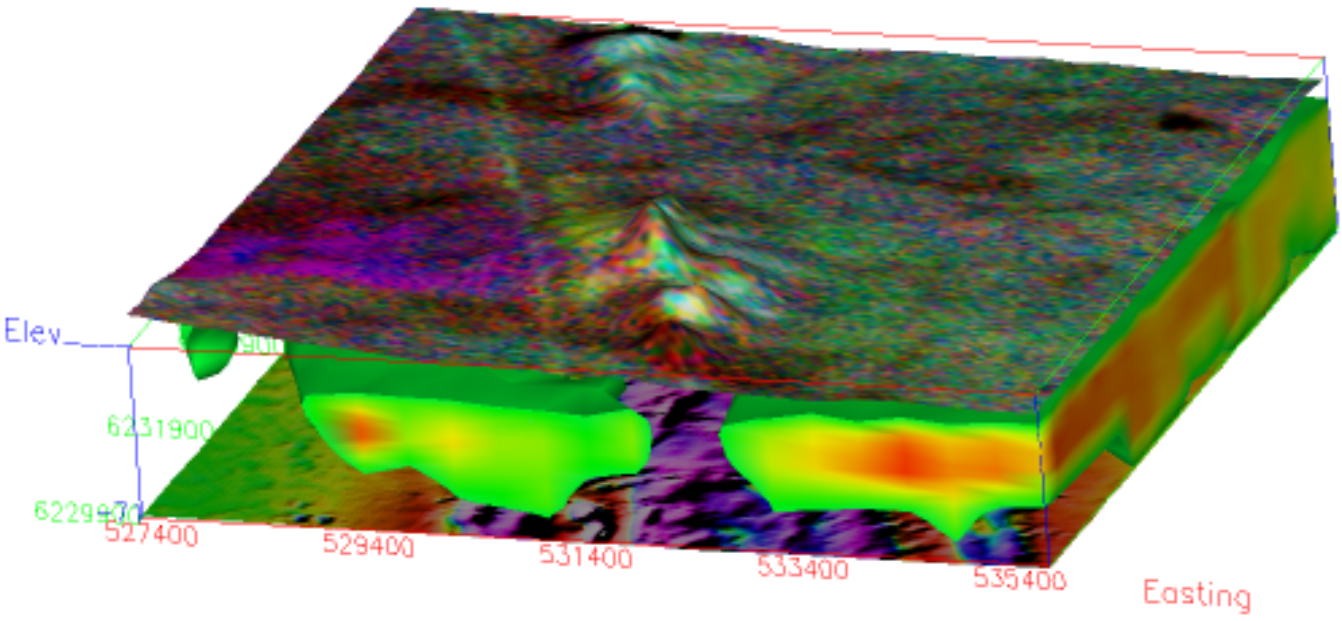

Fig. 22. A 3D block model displaying surface topography (DEM) and airborne gamma-ray spectrometric imagery over a conductivity plume derived from an airborne EM survey over the Gilmore area. An enhanced magnetic image at the bottom of the model provides a geological context. Areas of high conductivity (red hues) relate mainly to salt-bearing alluvial and colluvial sediments which have buried a palaeo-landscape with considerably more relief than the present day. The conductivity plume is clipped to show values greater than 500 mS/m.

interpolation techniques such as kriging create isosurfaces (3D surfaces of equal value) from scattered measurements (Fig. 18). The accuracy of such models depends on several factors — for example, drillhole sampling density and the level of interpretation built into the attributes being modelled. Widely spaced sample points will yield a more abstract, less accurate model than closely spaced sample observations. Such models can be generated from kriging either primary attributes (e.g., element concentration) or interpreted values or classes (e.g., transported or *in situ* zones within the regolith).

Building models based on interpreted attributes adds another source of potential error in the final image display. Inconsistencies in logging drillcore, for example, can be identified as random spikes in the 3D model (Fig. 18). Identifying errors highlights the use of 3D visualisation in checking data consistency and accuracy in databases. Similarly, assumptions built into simple geophysical models constructed to extract depth information from gravity, magnetic, and EM datasets are a potential source of error in the displayed image. Therefore, an understanding of the limitations of datasets being modelled, and the facility of representing any uncertainties in a display, are critical for assessing the accuracy and quality of the phenomena displayed.

Communicating with clients in 3D

Most geoscientific datasets are integrated and analysed in a GIS as thematic layers in 2D projections on paper or a computer screen. These themes are presented to clients as hardcopy outputs or as GIS datasets in either MapInfo- or ArcView-compatible formats. Communicating with clients in 3D is more of a challenge.

Displaying 3D information as static hardcopy products markedly degrades the information content and interactivity of the image being displayed. Preparing the information effectively for 3D visualisation requires the use of computer-generated depth clues — such as directed lighting, shading, and manipulation tools (e.g., resizing, rotating, etc.) — to create a dynamic 3D environment. Virtual reality takes the user–data interaction a step further by connecting and synchronising an image with the viewing direction of the user. This synchronicity is done by head-tracking display devices. Coupling the eye position with the image display provides a strong sense of reality and immersion or interconnectiveness between the user and the datasets being displayed. Despite active research in linking 3D GIS with a virtual-reality environment, the application of this technology to the wider community is still some way off. Currently 3D models are being provided to clients as:

- *Static image displays in standard image formats* (e.g., TIFF, MPEG, BMP).
- *Animated movie sequences*. Animations can be used to show temporal and non-temporal changes in spatial data. They effectively create dynamic displays by navigating through 2.5 (e.g., DEM image drape) or 3D models (e.g., fly-throughs, and migrating sections through 3D block models), and, for example, mapping hydrochemical pathways (water-table and solute fluctuations through time). They are presented to clients in either AVI or MPEG file formats, which can be readily viewed through PC multimedia players.
- *Virtual-reality modelling language (VRML) files*. Models saved as VRML files preserve the 3D integrity of an image, allowing the viewer to rotate, resize, and change illumination. VRML files can be viewed and manipulated via shareware Internet browsers and plug-ins. VRML files and animated movie sequences facilitate information dissemination to a wider client base (industry, general public, other scientists) and eliminate the dependence on specialised software to view and manipulate 3D objects.

Static images, animated files, and VRML files are also being incorporated as hotlinks with other spatially referenced maps and images in 2D GISs (ArcView). These linkages provide an important regional framework in which to interpret 3D models generated from district-scale datasets (e.g., mine-site and EM surveys).

Applications

The increasing importance of visualisation techniques for integrating and interpreting geoscientific information can be exemplified with reference to CRC LEME* regolith-focused studies in the Tanami (NT) and Gilmore areas (central NSW), and AGSO's modelling of environmental traces of sewerage discharge.

Regolith modelling

Understanding the regolith is important from an exploration perspective, because the surface expression of buried mineral deposits in highly weathered landscapes reflects its character and the physical and chemical dispersion processes that have operated in it. Regolith–landforms maps of the Tanami and Gilmore study areas are being complemented by 3D regolith and geochemical models over selected locations.

For Tanami, 3D regolith models derived from drillhole datasets incorporate gold geochemical plumes for visualising and resolving gold-dispersion trends from the mineralised host rock through the weathering profile to the surface (Fig. 19).

At Gilmore, surface mapping datasets (e.g., airphotos, airborne gamma-ray spectrometry, and DEM) provide only a partial understanding of regolith materials and associated geomorphic processes in a landscape buried by up to 70 m of Cainozoic alluvium and colluvium. Visualisation techniques integrating the surface datasets with subsurface (airborne magnetic, EM, waterbore, seismic profiling, and exploration drillhole) datasets (cf. Fig. 22) are elucidating the controls on metal and salt dispersion in the regolith and groundwater.

Chip and drillcore sample analysis distinguish regolith stratigraphy (e.g., sediments, saprolite, and saprock), mineralogy, geochemistry, and textures. Portable Infrared Mineral Analyser (PIMA) and downhole geophysical measurements (e.g., magnetic susceptibility and IP logs) reflect compositional, textural, and structural variations. These characters and properties are then modelled in 3D. Incorporating geochemical plumes in the 3D regolith models is helping to resolve metal dispersion from regolith-covered Au–Cu and epithermal Au deposits in the area.

Enhanced airborne magnetic data have effectively delineated palaeochannels containing maghemite pisoliths in the Gilmore area (Lawrie et al. 1999: AGSO Research Newsletter 30, 1–5). Integrating them with the 3D regolith models is helping to resolve the relationships between metal dispersion, palaeodrainage, and major structural trends (Fig. 20).

Regolith materials are an important source of soluble salt and control on salt mobility. Electrical conductivity maps derived from EM survey data can reveal areas of high salt concentration in the regolith. By incorporating conductivity and hydrogeochemical data in a 3D regolith framework, we can visualise the controls on salt distribution and movement in the landscape.

Sewerage-discharge traces

An environmental geochemical survey off Sydney in 1991 (Heggie et al. 1992: AGSO Research Newsletter 16, 23–24) recorded a suite of light hydrocarbons and temperature, salinity, and dissolved oxygen measurements at different depths in the water column. Methane, a unique tracer of sewerage discharges, characterised the hydrocarbons emanating from ocean outfalls.

Kriging of the geochemical data reveals the 3D geometry and locations of the anthropogenic hydrocarbon plumes (Fig. 21a, b). These hydrocarbon plumes are now being compared with 3D temperature and salinity models to better understand the controls on hydrocarbon dispersion.

Conclusions

The rapidly developing 3D visualisation technology is likely to play an increasingly important role in integrating, analysing, and resolving geoscientific information for constructing more robust exploration and environmental models. Visualisation techniques allow datasets from different disciplines (e.g., geomorphology, geochemistry, geophysics, hydrology, and spectral remote sensing) to be integrated, and

* The Cooperative Research Centre for Landscape Evolution & Mineral Exploration.

should encourage communication between staff in research teams.

The technology does have its limitations. Thus, the degree of extrapolation and abstraction of a model should be factored into the interpretation process. Again, sole reliance on the technology for interpretation can lead to an oversimplification of complex regolith and geological systems.

The use of 3D visualisation technology highlights the widening gap between hard-copy maps (2D) and interactive multimedia environments for communicating geoscientific information and concepts. However, visualisation and 3D modelling techniques are not an end-product themselves but a tool or process to solve a real problem.

[1] Minerals Division, Australian Geological Survey Organisation, GPO Box 378, Canberra, ACT 2601; tel. +61 2 6249 9455; fax +61 2 6249 9983; email john.wilford@agso.gov.au.

Evidence for possible zinc transport in hydrocarbon-bearing (C_1–C_9) fluids in the formation of Cobar-style deposits?

Kenneth C. Lawrie[1], Terrence P. Mernagh[1], Chris J. Boreham[2], & Graham A. Logan[2]

Thermal-decrepitation mass spectrometry has revealed extended-chain hydrocarbons (C_1–C_9) in premineralisation and early syn-Zn mineralisation veins at the Elura Ag–Pb–Zn mine (NSW). Laser Raman microprobe analysis demonstrates that the *n*-alkane signatures are from primary fluid inclusions in quartz and sphalerite. One hypothesis is that the hydrocarbons may be a component of a reduced, Pb–Zn–S-bearing low- to moderate-salinity fluid. The hydrocarbon components evolved to more mature compositions (C_1) through time. These data may have important implications for the transport of metals in low-temperature reduced connate fluids. The study has also confirmed that two fluids with dissimilar temperatures and redox properties (and salinities) were present throughout the pre- and synmineralisation vein paragenesis, and these data support a fluid-mixing model for the formation of the Elura deposit. The ore precipitated when hot, more oxidised low-salinity basement-derived fluids mixed with reduced, lower-temperature hydrocarbon-bearing basin-derived fluids. High-strain zones provided dilational sites for localising the deposit and for basin-scale conduits that tapped fluids from within the basin and underlying basement sources.

Fig. 23. An Elura hand specimen shows early crack–seal quartz (+sphalerite) veins (white) cross-cut by later sulphide-rich polymetallic veins. The host rock is silicified shale.

Introduction

Organic material (and/or hydrocarbons) is associated with some sediment-hosted base-metal deposits, including the Cobar deposits (Lawrie & Hinman 1999: AGSO Journal of Australian Geology & Geophysics, 17(4), 169–187; Lawrie et al. 1999: in C.J. Stanley et al., editors, 'Mineral deposits: processes to processing — proceedings of the fifth biennial SGA meeting and the tenth quadrennial IACOD meeting, London, 22–25 August 1999', A.A. Balkema, Rotterdam, 243–246). The overall sedimentary composition appears to be an important factor in controlling the redox character of basinal brines, and hence the capacity of these fluids to transport metals (Cooke et al. 1998: Geological Society of Australia, Abstracts, 49, 91). In basins whose sedimentary fill has buffered these brines to oxidised, near–neutral conditions, it has been proposed that metals are transported in oxidised sulphate-bearing fluids, and that redox reactions are responsible for ore precipitation (Barton 1967: Economic Geology, Monograph 3, 371–378). Metal destabilisation has been attributed to interaction with organic-rich host rocks (Hinman 1998: Geological Society of Australia, Abstracts, 49, 212; Broadbent et al. 1996: in T. Baker et al., editors, "MIC '96. New developments in metallogenic research: the McArthur–Mount Isa–Cloncurry minerals province. Extended abstracts", James Cook University of North Queensland [JCUNQ], Economic Geology Research Unit [EGRU], Contribution, 55, 24–27), or reduced sulphur at the trap site (Cooke et al. 1998: op. cit.). In those basins where reduced fluids are proposed, fluid mixing is viewed as the most likely ore-precipitation mechanism (Cooke et al. 1998: op. cit.).

Geological setting of the Cobar deposits

The Cobar deposits are structurally controlled epigenetic massive-sulphide and vein-style polymetallic Au–Cu–Ag–Pb–Zn orebodies hosted by the Late Silurian–Early Devonian Cobar Basin (NSW). This basin is an (inverted) intracontinental ramp basin filled mainly by siliciclastic marine turbidites and minor volcanics (Glen et al. 1994: Australian Journal of Earth Sciences, 41, 341–352). The deposits formed during Early Devonian inversion of the basin, and are localised within steeply dipping linear ductile high-strain zones towards its eastern margin (Glen 1985: Journal of Structural Geology, 7, 301–315). The host high-strain zones were also mixing zones and conduits for hydrothermal fluids.

The host rocks are generally metamorphosed to the chlorite grade, and, according to illite crystallinity data, reflect the transition between diagenesis and low-grade metamorphism adjacent to most deposits (Brill 1988: Australian Journal of Earth Sciences, 35, 295–302). Vitrinite reflectance data (R_0 3.3–12%; Schmidt 1980: MSc thesis, Australian National University; Robertson & Taylor 1987: Journal of Geochemical Exploration, 27, 77–101) suggest that the basinal strata were exposed to temperatures of burial diagenesis, but to hotter fluids in the high-strain zones (Robertson & Taylor 1987: op. cit.). Vitrinite reflectance data also show that organic material within and adjacent to the deposits was subject to intense thermal maturation well beyond the gas-generation window. This contrasts with Mississippi Valley-type deposits, whose adjacent host-rock kerogens are usually below the oil-generation window (Gize & Barnes 1994: in 'Sediment hosted Zn–

Pb ores', Springer-Verlag, New York, 13–26).

Previous studies have demonstrated that the genesis of Cobar deposits involved mixing fluids (Lawrie & Hinman 1999: op. cit.): one was moderately reduced and methane-bearing during mineralisation; another, basement-derived, was a more oxidised, CO_2-bearing, high-temperature, low-salinity fluid. Pb-isotope data suggest the Pb–Zn end-member of the mineralisation spectrum represents basinal-source dominance, whereas the Cu–Au mineralisation was basement-source dominant though still mixed (Lawrie & Hinman 1999: op. cit.).

The Cobar deposits are characterised by complex mineral parageneses. A six-stage paragenesis has been documented at the Elura Ag–Pb–Zn deposit in the northwest of the basin (Lawrie & Hinman 1999: op. cit., table 1a). Premineralisation veins comprise subhorizontal crack-quartz fibre veins, and anastomosing subvertical laminar and breccia quartz (± early sphalerite) veins (Fig. 23).

New data and results

Samples from several different premineralisation crack–seal and breccia veins (the latter containing sphalerite) were collected from within 10 m of the main sulphide orebodies at '3 drill level' in the Elura mine. The samples for laboratory analysis were obtained from mapped veins. Their structural and microstructural timing, and paragenesis, were resolved before fluid-inclusion studies.

Primary and pseudosecondary fluid inclusions in low-strain domains within euhedral quartz and sphalerite grains have a wide range of homogenisation temperatures (110–230°C), highly variable liquid–vapour ratios, and low to moderate salinities (2–5 wt% NaCl equivalent; Lawrie & Hinman 1999: op. cit.).

Laser Raman microprobe data

Laser Raman analysis (Dollish et al. 1974: 'Characteristic Raman frequencies of organic compounds', Wiley, New York) of primary and pseudosecondary inclusions has revealed hydrocarbon spectra in premineralisation quartz veins. The similarity of Raman spectra within individual crack–seal veins, and contrasts reflecting different hydrocarbon compounds in adjacent veins (Fig. 24a–c), suggest that the hydrocarbons were trapped during a moderately short time, and that individual crack–seal veins were active at slightly different times.

Saturated hydrocarbon components were identified in spectra obtained from primary liquid-rich inclusions within sphalerite from breccia veins (Fig. 24a). These data demonstrate the coexistence of Zn-rich and hydrocarbon-bearing fluids. The low salinity (<5% NaCl equiv.) of these fluids leaves open the possibility that metal transport involved organic species. Although the Raman data confirmed the presence of long-chain hydrocarbons within individual inclusions, and the spectra represent different compounds in discrete veins, the technique could not identify the individual hydrocarbon compounds owing to the degree of band overlap.

Where the early crack–seal veins are cross-cut by later high-temperature veins, or where veins are partially preserved near high-temperature deposits, the Raman spectra indicated possible pyrobitumens (Fig. 24c). These pyrobitumens may have formed by in-situ degradation of pre-existing hydrocarbon-bearing fluid inclusions.

The main stage of mineralisation was characterised by hydrocarbon-bearing fluids that contained variable proportions of CH_4 and CO_2 (Fig. 24d) and possible minor ethane (C_2H_6). The last stage of mineralisation at Elura was characterised by aqueous fluids with no detectable CH_4 or CO_2.

Thermal-decrepitation mass spectrometry

Thermal-decrepitation mass spectrometry (Hoffmann et al. 1988: Chemical Geology, 70, 287–299), which can identify various low-molecular-weight components (e.g., water, CO_2, and hydrocarbons), was applied to analyse the same premineralisation crack–seal quartz veins and early zinc in quartz veins analysed by the laser Raman technique.

According to Figure 25a, the contents of the inclusions were released over different time–temperature intervals, and two main groups can be recognised. They include large volumes of H_2O, CO_2, N_2, and hydrocarbons up to C_5H_{12} (Fig. 25b).

The components released at lower temperatures (group 1) consist mainly of *n*-alkanes with chain lengths $<C_9$ and minor H_2O, CO_2, and N_2 (Fig. 26a, upper part). The absence of longer chain *n*-alkanes may be

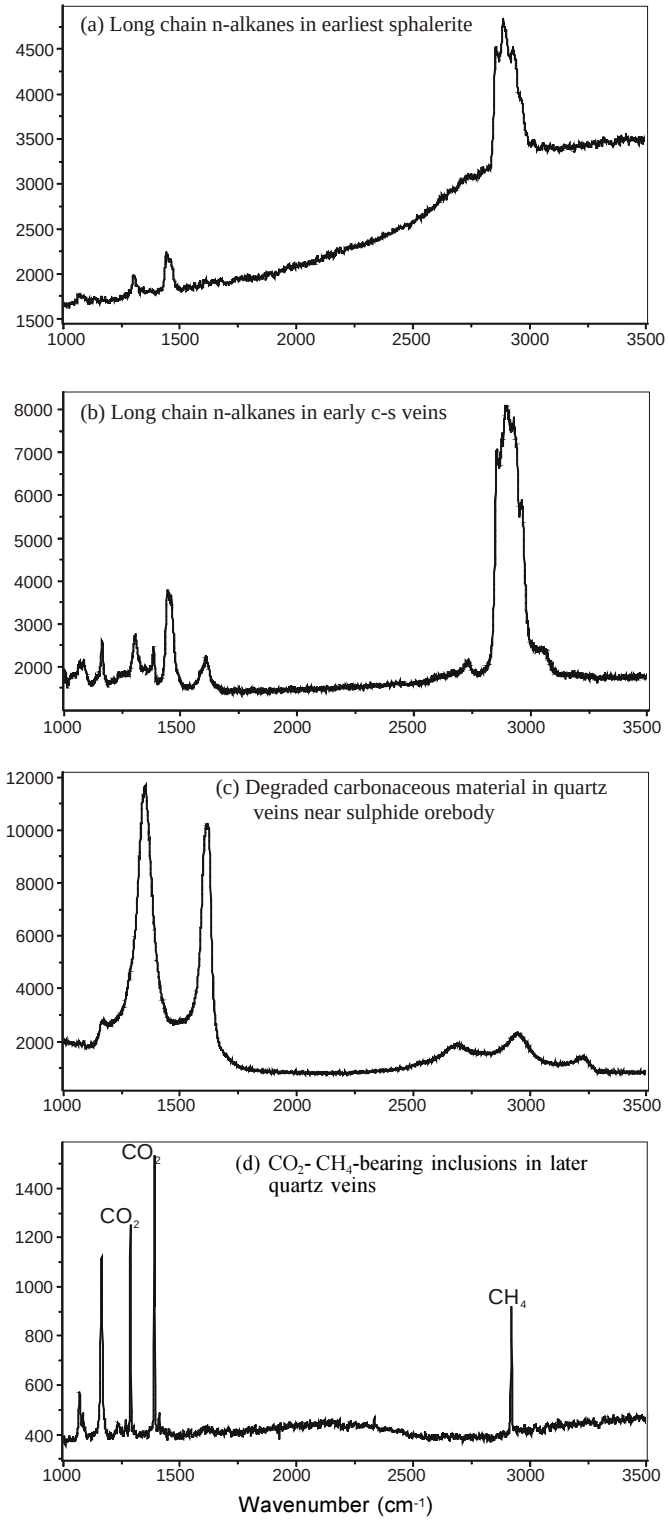

Fig. 24. Laser Raman spectra for fluid components within individual fluid inclusions: *n*-alkane spectra for liquid-rich primary inclusions within sphalerite (Fig. 24a) and quartz (Fig. 24b) from early quartz crack–seal veins; spectra for degraded carbonaceous material in quartz veins (Fig. 24c); and spectra for CO_2 and CH_4 in later quartz veins synchronous with polymetallic mineralisation (Fig. 24d).

a function of the sample volume and the limitations of the technique's sensitivity in detecting higher-molecular-weight hydrocarbons. The components released at higher temperatures (group 2; Fig. 26a, lower part) consist primarily of H_2O, CO_2, and N_2, and appear to lack the hydrocarbon distribution characteristic of group 1. These data are grouped together, and displayed against the data obtained from a blank sample for comparison (Fig. 26b).

These results are consistent with those from conventional fluid-inclusion studies (Lawrie & Hinman 1999: op. cit.), and show that two fluid components are present throughout the vein paragenesis at Elura. The data support the published fluid-mixing model containing two dissimilar fluids with contrasting temperatures and redox properties (Lawrie & Hinman 1999: op. cit; Lawrie et al. 1999: op. cit.).

Origin and role of hydrocarbons at Elura

An important question to be resolved is whether the hydrocarbons at Elura (and in the Cobar deposits generally) were externally derived from a deep basinal source, or locally produced as a result of the influx of hot metal-bearing fluids into organic-rich host-rocks. On the one hand, a deep basinal source may have offered the prospect of synchronous transport and complexing of zinc by hydrocarbons. On the other hand, a local hydrocarbon source, as proposed for the Century zinc deposit (Broadbent et al. 1996: op. cit.), may have contributed to an ore-depositional mechanism, as metal-rich fluids interacted with carbonaceous host rocks. Whereas a hydrocarbon contribution from local host rocks cannot be ruled out, evidence suggests that the hydrocarbons were largely derived from a much larger source than that in the local Cobar-deposit host-rock environment. The evidence includes:

- hydrocarbons are a component of the Cobar deposits regardless of the stratigraphic position of an ore deposit;
- individual orebodies are epigenetic, and highly discordant to the stratigraphy (e.g., the Elura deposit transects >1 km of thinly interbedded turbidites); hydrocarbons occur throughout an orebody's vertical extent and paragenesis, and neither they nor the orebodies are localised at the intersection with any lithology;
- host shear zones are narrow (<200 m at Elura) and host rocks (which include rhyolites at the nearby Peak deposit) have low TOC contents, raising doubts about their capacity to contribute the volume of fluid hydrocarbons estimated to occur in the deposits;
- host structures are basin-transecting, and contain evidence for premineralisation alteration assemblages that formed through interaction with organic acid-bearing reduced connate fluids (Robertson & Taylor 1986: op. cit.).

These observations suggest that the hydrocarbons in the premineralisation quartz veins and in the early syn-zinc mineral concentrations were not derived from local in-situ maturation of organic components, and that hydrocarbon-bearing fluids were generated on a large scale in the Cobar Basin. After the formation of the early crack–seal veins and the zinc mineralisation, small amounts of organic material in the high-strain inversion zones of the host lithologies interacted with the introduced fluids, which converted them to semi-anthracite or graphite synchronous with the later, hotter polymetallic mineralisation.

The data presented above suggest that the hydrocarbons are a component of a fluid expelled from deep within the basin. At all stages in deposit paragenesis, liquid:vapour ratios are highly variable within individual quartz grains, and a wide range of homogenisation temperatures, CO_2:CH_4 ratios, and salinities are apparent (Lawrie & Hinman 1999: op. cit.). Pb-isotope data (Lawrie & Hinman 1999: op. cit.) also suggest the presence of basinal- and basement-derived fluids carrying sulphur (Seccombe 1990: Mineralium Deposita, 25, 304–313; Sun & Seccombe 1998: Geological Society of Australia, Abstracts, 49, 433) and Pb–Zn components (Hinman 1992: PhD thesis, JCUNQ) derived from the host basin.

Host structures acted as basin-scale conduits that tapped fluids from both within the basin and from underlying basement sources (Seccombe 1990: op. cit.; Lawrie & Hinman 1999: op. cit.). The same structures acted as mixing zones for these contrasting fluids, and provided a focus for localising ore precipitation at dilational sites where basement heterogeneities permitted marked extension in high-strain volumes. The formation of the Cobar deposits links the physical effects of basin inversion (expressed as brittle–ductile deformation in restricted high-strain zones), the telescoping of geotherms, and the mixing of fluids from within the basin with those derived externally from the basement (Lawrie 1991: in 'Base metals symposium', JCUNQ, EGRU, Contribution, 38, 137–143; Hinman 1991: in 'Base metals symposium', JCUNQ, EGRU, Contribution, 38, 144–166).

Conclusions

This study has demonstrated the presence of *n*-alkanes (C_1–C_9) in premineralisation quartz veins and in early Zn-rich mineral concentrations at Elura. The preservation of free hydrocarbons in inclusions in veins, while carbonaceous matter in adjacent host rocks was degraded, is consistent with calculated stabilities which indicate that hydrocarbons may survive low-grade metamorphism (Mango 1991: Nature, 352, 146). Similar relationships have been noted in rocks metamorphosed to the prehnite–pumpellyite facies (Brocks et al. 1999: Science, 285, 103).

Preliminary calculations suggest that this early paragenetic association could represent organic complexing of zinc at low

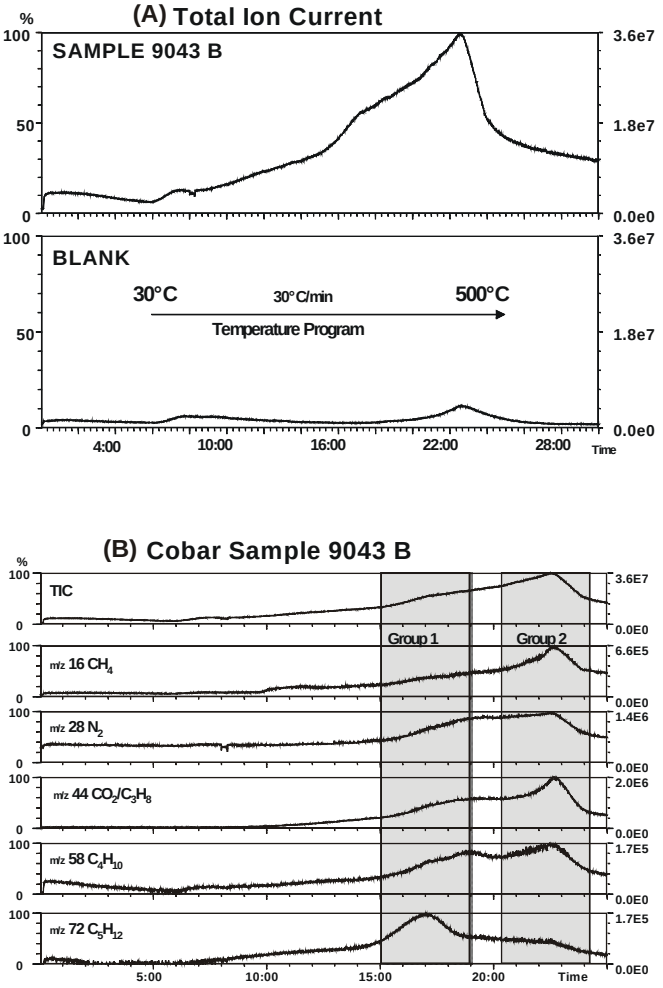

Fig. 25. Thermal-decrepitation mass spectrometry results for a quartz crack–seal vein. (A) Contents released from inclusions over different time–temperature intervals (top graph), and the output from a sample blank shown for comparison (lower graph). (B) Analysis of these data reveals two main groups, of which individual components (released during progressive heating) comprise large volumes of H_2O, CO_2, N_2, and hydrocarbons up to C_5H_{12}.

temperatures (D. Huston, AGSO, personal communication 1999). Furthermore, a genetic link between organo-sulphur compounds, and oilfield- and base-metal-deposit-forming (reduced) fluids has been suggested by some researchers (Sverjensky 1984: Economic Geology, 79, 23–37; Giordano 1985: in Geological Society of London, Special Publication 78, 175–202; Sicree & Barnes 1996: Ore Geology Reviews, 11, 105–131; Kharaka et al. 1998: Reviews in Economic Geology, 9). An alternative hypothesis is that the early mineralisation resulted from the mixing of pulses of zinc-rich fluids and cooler hydrocarbon-bearing fluids generated at different depths in the basin.

A progressive (or episodic) shift to higher methane and C_2 hydrocarbon contents with increasing salinity and temperature (in the reduced fluid component) is apparent through time. This is consistent with a connate source for the hydrocarbon-bearing fluid, which was expelled from the basin in response to tectonic inversion and prograde thermal maturation of the basin sediments. Similar hydrocarbon-bearing fluids have been reported in epigenetic Zn-rich mineralisation in the Coeur d'Alene base- and precious-metal veins in the USA (Leach et al. 1988: Geology, 16, 122–125).

Acknowledgments

We thank Karl Adamson for carrying out the solid-probe mass-spectrometric analysis; Mark Hinman for hours of stimulating discussions on the formation of the Cobar deposits; David Huston, Jim Jackson, and Tony Yeates for constructive reviews of the manuscript; Tony Yeates also for providing funds from AGSO's Onshore Petroleum Basins Program for sample preparation and analysis; and AGSO's Chiefs of Divisions and Chief Executive Officer for encouraging cross-divisional research.

[1] Minerals Division, Australian Geological Survey Organisation, GPO Box 378, Canberra, ACT 2601, Australia; tel. +61 2 6249 9847 (KCL), +61 2 6249 9640 (TPM); email ken.lawrie@agso.gov.au, terry.mernagh @agso.gov.au.

[2] Petroleum & Marine Division, Australian Geological Survey Organisation, GPO Box 378, Canberra, ACT 2601, Australia; tel. +61 2 6249 9488 (CJB), +61 2 6249 9460 (GAL); email chris.boreham@agso.gov.au, graham.logan@agso.gov.au.

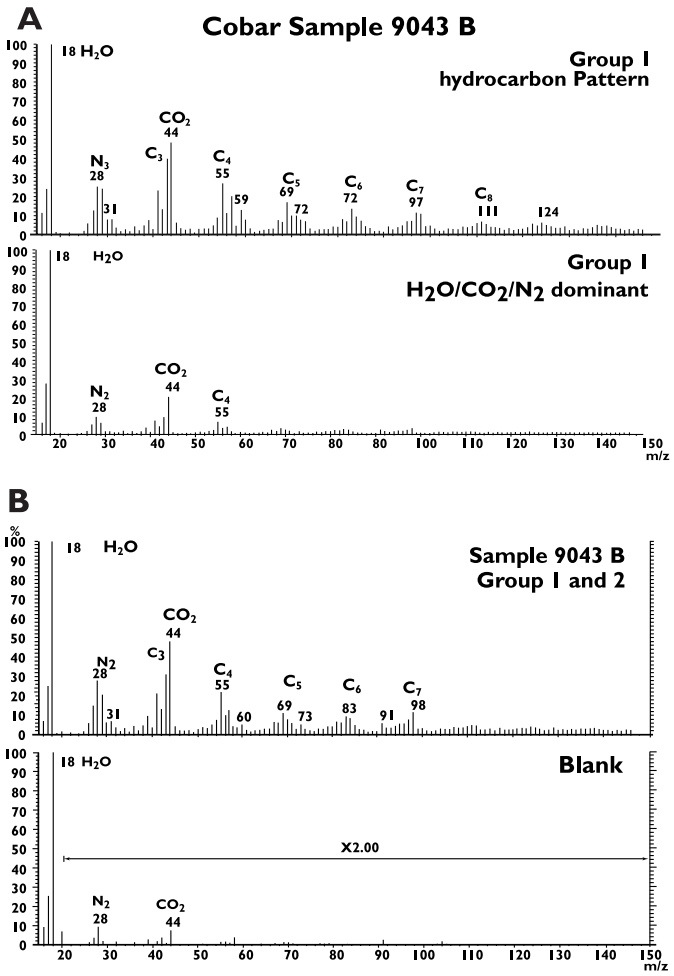

Fig. 26. Further thermal-decrepitation mass spectrometry results for the same quartz crack–seal vein. The group 1 components (released at low temperatures; A, top graph) are mainly hydrocarbons with chain lengths <C_9 and minor H_2O, CO_2, and N_2. The components released at higher temperatures (group 2; A, lower graph) consist primarily of H_2O, CO_2, and N_2. Data from groups 1 and 2 are combined (B, top graph), and compared with the components from a sample blank, which provides a baseline comparison (B, lower graph).

Preliminary AGSO scheme for standard database entry of sequence stratigraphic units

Albert T. Brakel[1] & Vicki Passlow[1]

To address the urgent problem of entering sequence stratigraphic units into AGSO's databases, a preliminary scheme for standarised database entry of these units has been drawn up and is being tested. This scheme focuses on those aspects that are the particular immediate concern of our databases, namely the definition and naming of these units. It does not deal with other aspects of sequence units such as Vail–Exxon vs Galloway-type units, or the basis for ranking units in hierarchies. The aim is to provide a quick result to fulfil immediate needs, and to be able to enter those units already published or about to be published. In the longer term, moves are under way to reach consensus on a national scheme for standards in the definition and naming of these units (Brakel 1999: APPEA Journal, 39(1), 485–493), but if this eventually produces a different scheme, the existing units in the databases can be linked to the new conventions. Comments from industry on the preliminary AGSO scheme are welcome.

Principles

The scheme is based on the following principles:

1. Formally define all sequences in a way similar to lithostratigraphic units but with variations that are peculiar to sequences — e.g., representative or type localities for sequence boundaries that can include outcrops, seismic line locations, and/or well intervals; biostratigraphic constraints; and methodology.
2. Use sequence boundaries as the defining parameters for sequence units (not type sections, lithology, etc.).
3. Names for sequences must be unique, and distinguishable from lithostratigraphic units.

4. Names of 1st-, 2nd-, and 3rd-order units must be proper names, not alphanumeric codes.
5. Use a digital hierarchy for subsequences and higher-order units — e.g., Dingo 1.2.3.
6. Avoid names that are age-specific — e.g., *M. australis* Sequence.
7. Preferably avoid naming the sequence boundary.
8. Allow the abbreviation of associated formation names — e.g., a sequence that contains mainly Riversleigh Formation strata can be called the River Sequence.
9. Allow the use of geographic names, including well names.
10. Invent other appropriate names that do not contravene the other rules. This will be particularly useful in areas where no names at all exist.
11. A term such as 'Sequence', 'Supersequence', 'Megasequence', etc., must always be attached to the name of a sequence stratigraphic unit.
12. Store the parent unit of a sequence unit in an appropriate database.
13. Record a standard abbreviation in the database for use when names are too long for maps, sections, etc.

Hypothetical example of how a sequence could be defined

Name and rank: White Gull Sequence
Derivation: White Gull 1 well, at lat. 11°30'S, long. 140°30'E.
Synonymy (if any): Upper part of Vindaloo Sequence of Jones (1985).
Distribution: Wildcat Basin, except for the NE side where it has been eroded away.
Lower bounding surface:

Type locality: Depth of 1532 m in the White Gull 1 well, which corresponds to SP551, TWT 498 ms in seismic section AZCO 1996–3.

Identifying features: 8° dip discordance on dipmeter log, strong spike on gamma-ray log, stratal termination surface in seismic section AZCO 1996–3.

Adjacent lithologies at the type locality: Limestone below the boundary, mudstone above.

Lithostratigraphic units at the type locality: Johns Limestone below, Bintang Formation above.

Age of rock below: Valanginian, *E. torynum* Zone.

Age of rock above: Valanginian, S. *areolata* Zone.

Regional aspects: Angular discordance decreases towards the centre of the basin.

Upper bounding surface:

Type locality: Depth of 1102 m in the White Gull 1 well, which corresponds to SP551, TWT 365 ms in seismic section AZCO 1996–3.

Identifying features: 3° dip discordance on dipmeter log, strong spike on gamma-ray log, stratal termination surface in seismic section AZCO 1996–3.

Adjacent lithologies at the type locality: Mudstone below the boundary, sandstone above.

Lithostratigraphic units at the type locality: Bintang Formation below, Dugong Formation above.

Age of rock below: Valanginian, S. *areolata* Zone.

Age of rock above: Valanginian, S. *tabulata* Zone.

Regional aspects: Becomes a correlative conformity in the centre of the basin.

Sequence regional aspects: Subaerially deposited sandstone-dominated succession along the eastern basin margin interfingers with paralic mudstone and sandstone westwards, and passes farther west into deep offshore mudstone-dominated rocks. Sequence thickens towards the palaeoshelf margin, but thins again in the deeper-water facies.
Constituent units: Composed of three 4th-order units, the White Gull 1 Subsequence, White Gull 2 Subsequence, and White Gull 3 Subsequence.
References:

Jones, W.H., 1985. A sequence framework for the Cretaceous of the Wildcat Basin. *Drill Here Journal*, 63, 119–137.

Example of naming sequences

The naming of sequences, both in AGSO and elsewhere, has been based in the past on a number of methods, most of which are inappropriate to the standards set out here. Names are typically non-unique and are commonly based on alphanumeric codes or age-specific names. Use of the geographic parts of formally defined lithostratigraphic names is also widespread. Ideally, only where a sequence stratigraphic unit and a lithostratigraphic unit are identical should the geographic name also be adopted. In practise the units are often not identical, but such usage is nevertheless common in the literature.

An example from the Browse Basin of how current usage might be revised is set out below according to the preliminary AGSO scheme. Alongside the published version is a possible revised scheme, which follows the principles identified herein. This revised scheme is based on well names. Where feasible, sequence names are derived from the reference well for that sequence.

Browse Basin sequence stratigraphy

Published scheme	*Possible revised scheme*
BB12	Arquebus Sequence
BB12C	Arquebus 3 Subsequence
BB12B	Arquebus 2 Subsequence
BB12A	Arquebus 1 Subsequence
BB11	Heywood Sequence
BB10	Caswell Sequence
BB9	Shell Sequence
BB8	Sheherazade Sequence
BB7	Perindi Sequence
BB6	Lacepede Sequence
BB5	Brecknock Sequence

Call for comments

The AGSO scheme should be compatible with industry methods of storing such data. We are therefore asking for industry feedback on this scheme, and greatly value any comments (positive or negative) that you can give us. Is this a practical way of handling the type of data your company deals with? If not, what changes should be made?

Please address your comments to us at the postal or email addresses annotated in the footnote below.

Acknowledgments

This preliminary scheme reflects the input of an ad hoc committee consisting of John Bradshaw, Jim Jackson, John Kennard, Cathy Brown, Frank Brassil, and the two of us.

[1] Minerals Division (AB), Petroleum & Marine Division (VP), Australian Geological Survey Organisatiuon, GPO Box 378, Canberra, ACT 2601; tel. +61 2 6249 9697 (AB), +61 2 6249 9558 (VP); fax +61 2 6249 9971 (AB); email albert.brakel@agso.gov.au, vicki.passlow@agso.gov.au.

New age constraints for Cu–Au(–Mo) mineralisation and regional alteration in the Olary–Broken Hill region

Roger Skirrow[1], Roland Maas[2], & Paul Ashley[3]

The Curnamona Province, including the Broken Hill Domain and its giant Pb–Zn–Ag deposit, is emerging as a significant Cu–Au(–Mo) province owing to the recent discoveries of the Portia, White Dam, and Kalkaroo prospects. New $^{40}Ar/^{39}Ar$ data for hydrothermal muscovite at the Mundi Mundi Cu–Au prospect, hosted by <1720-Ma metasediments, implies a minimum age of ~1500 Ma for Fe-oxide–associated Cu–Au mineralisation. In conjunction with key geological and geochemical signatures, this Mesoproterozoic constraint enhances the potential of the Curnamona Province as a host to Cu–Au–Fe systems similar to those at Olympic Dam and/or Cloncurry–Tennant Creek.

A novel dating technique — single-mineral step-leach analysis of Pb isotopes — applied to date titanite associated with

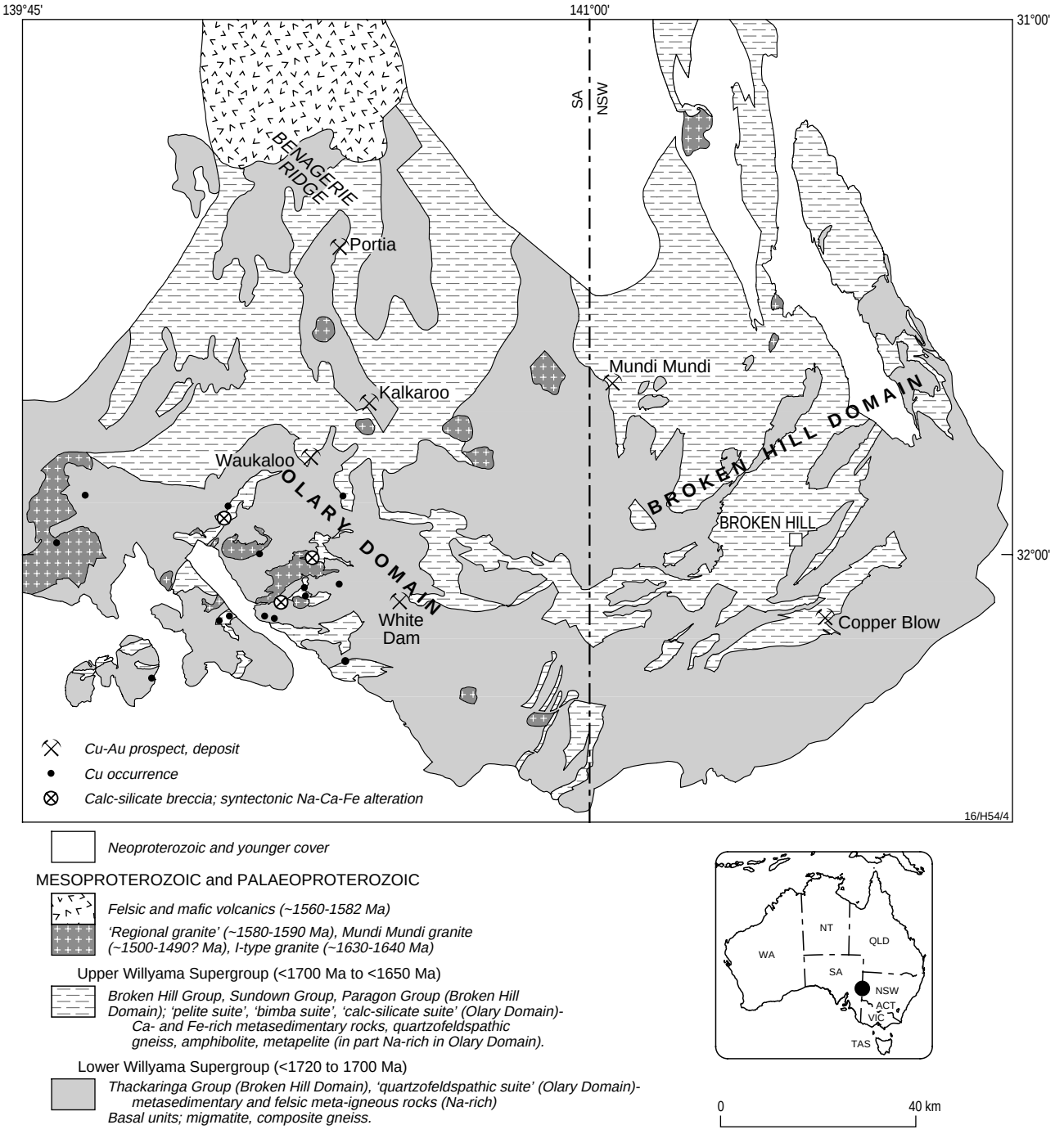

Fig. 27. Simplified geology of part of the Curnamona Province (after Laing et al. 1996: 'Interpreted solid geology of the Curnamona Province, 1:500,000 scale', Department of Mines & Energy, South Australia).

syntectonic regional Na–Ca–Fe metasomatism has yielded a $^{207}Pb/^{206}Pb$ isochron age of 1660 ± 33 Ma. Although this alteration may represent earlier and/or deeper-level high-temperature hydrothermal activity relative to Cu–Au(–Mo) deposition, it is indicative of a regional-scale flux of fluids with a metal-carrying capacity. As such, it is viewed as a positive factor for the prospectivity of Fe-oxide-associated Cu–Au(–Mo) in the province.

As part of the Broken Hill Exploration Initiative* (BHEI), AGSO is leading a multidisciplinary study of the Cu–Au(–Mo) metallogenic framework of the Curnamona Province. This study is applying geological, geochemical, stable-isotopic, and geochronological methods to resolve the timing and key components of Cu–Au mineralising systems, and relationships with regional alteration zones. Recently acquired high-resolution aeromagnetic, gravity, and gamma-ray spectrometric datasets provide the basis for a new perspective on the metallogeny and prospectivity of this largely concealed terrane.

Cu–Au(–Mo) mineralisation

Palaeoproterozoic metasediments of the Willyama Supergroup host a range of epigenetic Cu–Au(–Mo) systems of growing exploration significance, as well as numerous prospects of stratabound Ba, Zn, Pb, Ag, and Co (Fig. 27). Copper–gold deposits in the Olary Domain occur within a few hundred metres of the interface between the 'pelite suite' (upper part: ≤1650 Ma; Page et al. 1998: in AGSO Record 1998/25, 89–93) and underlying calc-silicate-rich metasediments of the 'Bimba suite' and 'calc-silicate suite' (informal stratigraphic nomenclature after Clarke et al. 1986: Precambrian Research, 34, 107–137). Felsic volcanics and ?sills within the lower parts of the 'calc-silicate suite' and underlying 'quartzofeldspathic suite' were emplaced at <1720–1700 Ma (Fig. 28; Ashley et al. 1996: Lithos, 38, 167–184; Page et al. 1998: op. cit.).

The Olary Cu–Au(–Mo) systems are broadly stratabound, although the disseminated and stockwork deposits are locally transgressive to compositional layering, and partly fracture- or fault-controlled. The larger Cu–Au(–Mo) systems are associated with hydrothermal magnetite ± hematite (except White Dam; see below), and the Copper Blow deposit in the Broken Hill Domain occurs in a shear-related magnetite ironstone (Skirrow & Ashley 1998: in AGSO Record 1998/25, 104–108). Microstructural and paragenetic observations at the Mundi Mundi Cu–Au prospect and other deposits indicate multiple generations of magnetite crystallisation, including disseminated premineralisation and later syndeformational hydrothermal stages. Some if not all Cu–Fe sulphide and Au mineralisation was associated with this hydrothermal magnetite and attendant potassic alteration, which includes combinations of reddish K-feldspar or albite, biotite, carbonate, amphibole, quartz, and uncommon muscovite. Late-stage chloritisation of hydrothermal biotite was widespread throughout the northern Olary region. Minor late veins of carbonate–quartz–chlorite ± fluorite ± chalcopyrite ± barite are common in the Benagerie Ridge area.

The White Dam deposit is distinguished from most other Olary Cu–Au(–Mo) systems by higher Au/Cu ratios and by very low iron-oxide content (McGeogh & Anderson 1998: in AGSO Record 1998/25, 69–71). Gold and disseminated molybdenite, chalcopyrite, and pyrite are localised partly within quartzofeldspathic veins/segregations in quartz–feldspar–biotite gneiss.

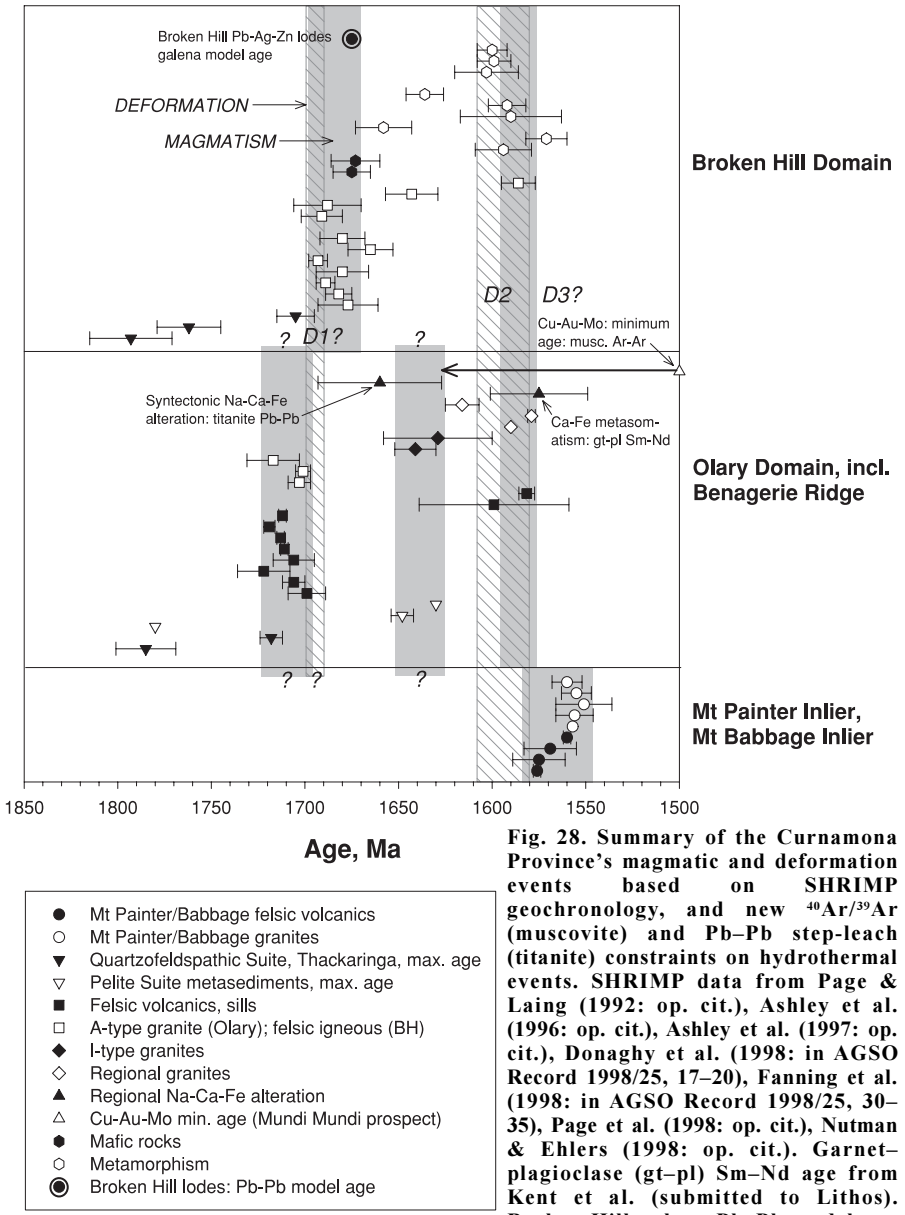

Fig. 28. Summary of the Curnamona Province's magmatic and deformation events based on SHRIMP geochronology, and new $^{40}Ar/^{39}Ar$ (muscovite) and Pb–Pb step-leach (titanite) constraints on hydrothermal events. SHRIMP data from Page & Laing (1992: op. cit.), Ashley et al. (1996: op. cit.), Ashley et al. (1997: op. cit.), Donaghy et al. (1998: in AGSO Record 1998/25, 17–20), Fanning et al. (1998: in AGSO Record 1998/25, 30–35), Page et al. (1998: op. cit.), Nutman & Ehlers (1998: op. cit.). Garnet–plagioclase (gt–pl) Sm–Nd age from Kent et al. (submitted to Lithos). Broken Hill galena Pb–Pb model age (errors unknown) from Sun et al. (1994: op. cit.). 1690–1700-Ma age of D1 based on Gibson (1998: in AGSO Record 1998/25, 38–40).

* A collaborative National Geoscience Mapping Accord project involving AGSO, Primary Industries & Resources South Australia (PIRSA), and the New South Wales Department of Mineral Resources (DMR).

Regional alteration

Regionally extensive zones of alteration are prominent in both the Olary and Broken Hill Domains (Ashley et al. 1997: Mines & Energy, South Australia, Report Book 97/17; Ashley & Plimer 1998: Geological Society of Australia, Abstracts, 49, 14). Styles include pre- or early tectonic sodic metasomatism in both domains; and syntectonic Na–Ca–Fe alteration, garnet ± epidote replacements, and potassic–iron-oxide–carbonate alteration, which are confined mainly to the Olary Domain (Skirrow & Ashley 1998: op.cit.). The effects of pre- or early tectonic sodic metasomatism are largely stratabound and pervasive within the quartzo-feldspathic, calc-silicate and lower pelite suites in the Olary Domain, and within the Thackaringa Group in the Broken Hill Domain (Fig. 27). They are overprinted by fabrics associated with D_2 in the scheme of Clarke et al. (1986: op. cit.). Abundant disseminated magnetite ± pyrite in some sodic plagioclase-rich ('albitite') assemblages reflects coupled Na–Fe metasomatism during this early alteration.

The products of syntectonic Na–Ca–Fe alteration overprint the early sodic metasomatic effects. Accordingly, albite ± clinopyroxene ± amphibole ± garnet vein networks and calc-silicate-matrix breccias occur widely and preferentially within the calc-silicate suite (e.g., Cathedral Rock; Yang & Ashley 1994: 'Proceedings of the AMF symposium on Australian research in ore genesis', Australian Mineral Foundation, Adelaide, 16.1–16.5). The matrix of the breccias is composed of clinopyroxene and/or amphibole ± albite ± titanite ± quartz ± magnetite ± hematite. Clasts and host rocks are intensely albitised within tens to hundreds of metres of breccia bodies. These Na–Ca–Fe alteration effects were localised by upright folding and brittle–ductile shearing, and at least in part postdate ~1630–1640-Ma I-type granites, yet are cut by granite dykes affiliated(?) with the minimally altered ~1580–1590-Ma 'regional granite' suite (Fig. 28). The relationship of the syntectonic Na–Ca–Fe alteration to metasomatic zones of massive garnet ± epidote ± plagioclase (1575 ± 27 Ma, Sm–Nd; Kent et al. submitted to Lithos) is unclear at present. Fluids involved in the formation of calc-silicate-matrix breccias and garnet-rich alteration zones were generally oxidised hot (450–550°C) hypersaline brines capable of leaching and transporting metals (Yang & Ashley 1994: op. cit.; Ashley & Plimer 1998: op. cit.; R.G. Skirrow & P. Ashley, unpublished data).

New geochronological results

Muscovite with grainsize 0.2–1.0 mm separated from gold-bearing quartz–magnetite–chalcopyrite–K-feldspar veins cutting upper-greenschist–lower-amphibolite-facies Palaeoproterozoic pelitic and albitite rocks at the Mundi Mundi prospect (Fig. 27) yielded a disturbed $^{40}Ar/^{39}Ar$ spectrum with a total fusion age of 1496 ± 9 Ma (Fig. 29). Although this spectrum is complex, we may infer that initial closure to argon loss occurred before ~1500 Ma. This age is considered a minimum for vein formation and Cu–Au introduction. The oldest apparent age steps suggest a >1500-Ma component of uncertain origin. Thermal disturbance after ~1350 Ma has resulted in young initial steps. The source of the disturbance may have been the Delamerian Orogeny (520–450 Ma), which resulted in widespread resetting of $^{40}Ar/^{39}Ar$ ages farther south, west, and east in the Olary Domain (Bierlein et al. 1996a: Mineralogy & Petrology, 58, 1–22) and Broken Hill Domain (Harrison & McDougall 1981: Earth and Planetary Science Letters, 55, 123–149) but apparently had less effect in the Mundi Mundi prospect area.

Titanite in syntectonic calc-silicate-matrix breccia has been dated by the Pb step-leach technique for single minerals (cf. Frei & Kamber 1995: Earth and Planetary Science Letters, 129, 261–268). A titanite separate was treated with nitric acid in five steps ranging from 10 minutes to 15 hours, and the residue dissolved in hydrofluoric acid. Ludwig's (1989: US Geological Survey, Open File Report OF–88–0557) software resolved a five-point $^{207}Pb/^{206}Pb$ isochron age of 1660 ± 33 Ma (MSWD 5.8; HNO_3 steps). This preliminary result suggests that a regional-scale Na–Ca–Fe metasomatic and deformation event predated the ~1600-Ma peak of the Olarian orogeny (Page & Laing 1992: Economic Geology, 87, 2138–2168). Further work is in progress to verify the Pb–Pb result. A U–Pb zircon ion-probe age of 1641 ±11 Ma for I-type 'tonalite' in the Olary Domain (Ashley et al. 1997: op. cit.), which is overprinted by the effects of calc-silicate alteration and brecciation, provides a possible maximum age for this style of alteration. Correlation of I-type magmatism with the 1640–1660-Ma metamorphic–deformation event postulated by Nutman & Ehlers (1998: Precambrian Research, 90, 203–238) in the Broken Hill Domain remains problematical (Fig. 28).

Implications for Cu–Au(–Mo) exploration

Knowledge of the absolute timing of Cu–Au(–Mo) mineralisation in the Curnamona Province is critical to exploration models, yet there have been few geochronological constraints. Copper–gold deposits occur in Adelaidean sequences in the region, implying at least some mobilisation of Cu–Au after ~800 Ma. Based on $^{40}Ar/^{39}Ar$ dating,

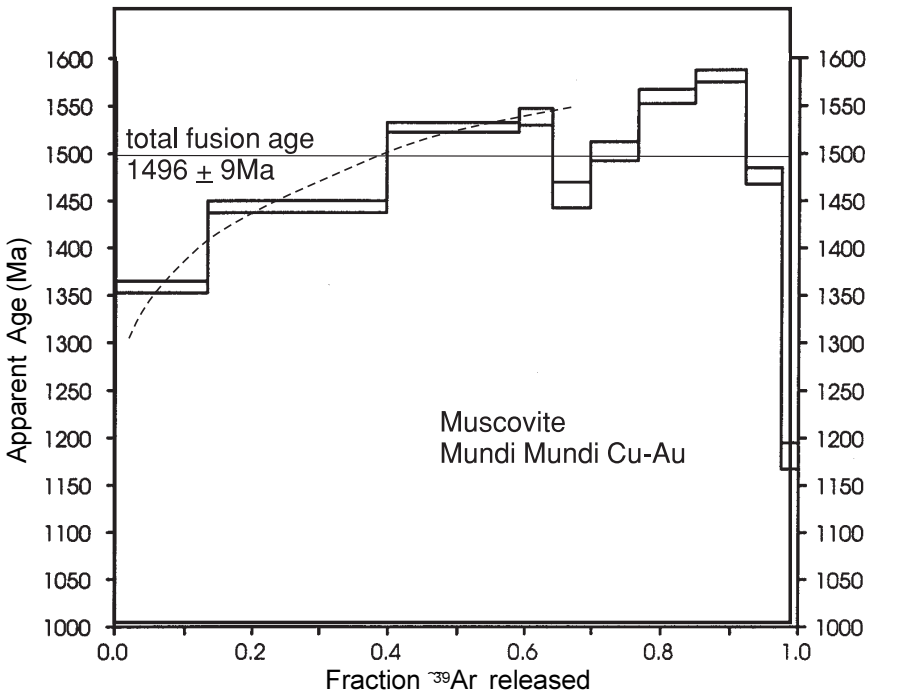

Fig. 29. $^{40}Ar/^{39}Ar$ step-heating spectrum for hydrothermal muscovite associated with Cu–Au mineralisation, Mundi Mundi prospect (Fig. 27). Widths of apparent age steps are 1-σ errors.

Bierlein et al. (1996a: op. cit.) proposed that epigenetic Cu–Au–quartz and Pb–Zn ± Cu-carbonate vein deposits in the Olary Domain were emplaced during the Delamerian Orogeny. By comparison, lead-isotope signatures of least-radiogenic galena and Fe-, Zn-, and Cu-sulphides in stratabound and epigenetic mineralised veins in the Olary Domain are consistent with the Meso–Palaeoproterozoic Pb-isotope signature of the Broken Hill orebody (Sun et al. 1994: AGSO Research Newsletter 24, 19–20; Bierlein et al. 1996b: Australian Journal of Earth Sciences, 43, 177–188; Lawie et al. 1997: Geological Society of Australia, Abstracts, 44, 44).

The $^{40}Ar/^{39}Ar$ data for Mundi Mundi are a further indication of a Mesoproterozoic (or older) age for Cu–Au mineralisation in the Curnamona Province, corroborating earlier suggestions based on geological evidence (e.g., Ashley & Plimer 1998: op. cit.) and lead isotopes (Bierlein et al. 1996b: op.cit.). Several key components of Proterozoic Cu–Au–Fe mineral systems are present in the Curnamona Province: (i) ~1580–1590-Ma granitoids resembling the Hiltaba Suite (Wyborn et al. 1998: in AGSO Record 1998/25, 123–126), (ii) abundant hydrothermal magnetite and hematite, (iii) Cu–Au(–Mo) association and anomalous LREE, Ba, and F (R.G. Skirrow, unpublished data), (iv) potassic, 'red rock', and precursor Na–Ca–Fe regional alteration, and (v) syn- to late tectonic timing of at least some Cu–Au deposition (Conor 1996: in W.V. Preiss, compiler, "Resources '96 Convention", Mines & Energy, South Australia, Abstracts, 40–41; Skirrow 1999: in C.J. Stanley et al., editors, 'Mineral deposits: processes to processing — proceedings of the fifth biennial SGA meeting and the tenth quadrennial IACOD meeting, London, 22–25 August 1999', A.A. Balkema, Rotterdam, 1361–1364). In conjunction with these characteristics, the ~1500-Ma minimum age of Cu–Au provides further support for Olympic Dam-style mineralisation (~1590 Ma; Johnson & Cross 1995: Economic Geology, 90, 1046–1063) and/or Cloncurry–Tennant Creek-style Cu–Au–Fe mineral systems in the Curnamona Province.

Acknowledgments

We thank our BHEI colleagues, and especially Colin Conor (PIRSA), for their contributions in the field and for fruitful discussions. David Foster (La Trobe University) determined the $^{40}Ar/^{39}Ar$ step-heating analyses. BHP Discovery, Platsearch NL, Savage Resources, MIM Exploration, Placer, Newcrest Mining, Rio Tinto Exploration, and Eaglehawk Geological Consulting kindly provided access to drillcore. Titanite and muscovite mineral separates were prepared at AGSO and Monash University.

[1] Minerals Division, Australian Geological Survey Organisation, GPO Box 378, Canberra, ACT 2601; tel. +61 2 6249 9442; fax +61 2 6249 9983; email roger.skirrow@agso.gov.au.

[2] Department of Earth Sciences, La Trobe University, Bundoora, Vic. 3083; tel. +61 3 9479 2490; email R.Maas@latrobe.edu.au.

[3] Division of Earth Sciences, University of New England, Armidale, NSW 2351; tel. +61 2 6773 2860; fax +61 2 6773 3300; email pashley@metz.une.edu.au.

Geochemical characteristics of ca 3.0-Ga Cleaverville greenstones* and later mafic dykes, west Pilbara: implication for Archaean crustal accretion

Shen-su Sun[1] & Arthur H. Hickman[2]

Different tectonic settings proposed for greenstones in the Cleaverville area, west Pilbara, include Archaean oceanic crust in an accretionary complex, oceanic island arc, and intraplate rift. The geochemistry of these greenstones and that of later mafic dykes offers insights to the crustal accretion and changes of tectonic environment with time in this area.

In a previous AGSO Research Newsletter (1998: 28, 25–28), we reported new Nd-isotope and chemical data for felsic and mafic igneous rocks from the west Pilbara. Combined with geochronological data, these data support a model in which juvenile crust formed at different times in the east and west Pilbara Craton in response to plate tectonics and terrane accretion.

Stratigraphic synopsis, Cleaverville area

In the Cleaverville area (east of Karratha; Fig. 30), greenstones with mid-ocean-ridge basalt (MORB) affinities (Regal Formation), and ~3020-Ma felsic volcanic rocks (Cleaverville Formation) with young Nd T_{DM} model ages (3110–3210 Ma), apparently represent juvenile crust. According to Hickman (1997: Geological Survey of Western Australia [GSWA], Annual Report, 76–81), these rocks have depositional ages of ≥3020 Ma (Cleaverville Formation) and ≥3050 Ma (Regal Formation). Over much of the west Pilbara, the Regal Formation stratigraphically underlies the Cleaverville Formation (mostly chert–banded iron formation (BIF) and clastic rocks); the contact is conformable and unfaulted in several places. The Regal Formation is generally in tectonic contact with the 3260-Ma Nickol River Formation, Ruth Well Formation, and Karratha Granodiorite. The entire succession is loosely constrained between 3020 and 3260 Ma. One of us (AHH) considers that the Regal Formation (with MORB-like basalts) has been thrust across the 3260-Ma units, apparently from the northeast.

Cleaverville greenstone genesis: conflicting views

Pillow basalts in the Regal Formation greenstone succession were previously interpreted to have been deposited in an intraplate setting. This view was challenged several years ago as a result of 1:5000 field mapping (unpublished) by Y. Isozaki and his Tokyo Institute of Technology colleagues. Based on their extensive field experience with modern accretionary complexes (e.g., Isozaki et al. 1990: Tectonophysics, 181, 179–205; Isozaki & Blake 1994: Journal of Geology, 102, 283–296), Isozaki et al. (1991: EOS, 72, 542) interpreted this sequence as tectonically repeated slices of oceanic crust separated by multiple layer-parallel faults in an accretionary complex generated by subduction of oceanic lithosphere. After a recent visit to the Cleaverville area, R. Blewett (AGSO,

* The expression 'Cleaverville greenstones' refers to greenstones in the Regal Formation in the Cleaverville area.

personal communication 1999) suggested that the presence of melange, subsequently folded and sheared, may support their hypothesis.

Low-grade greenstones of the Regal Formation in the Cleaverville area were previously studied by Glikson et al. (1986: BMR/AGSO Record 1986/14) and Ohta et al. (1996: Lithos, 37, 199–221). Ohta et al. reported a large variation in Nb/Th (5–60, mostly 5–10) and considerable depletion of Nb (Nb/La=0.4-0.6) for Cleaverville MORB-like basalts with only slightly light REE-depleted patterns. They interpreted this apparent depletion in Nb to core formation. They also attributed a high estimate of total iron in the mantle source of the Cleaverville greenstones relative to pyrolite mantle as a result of incomplete core formation in the early Archaean. This contradicts their interpretation of Nb depletion in their samples.

Ohta et al. suggested that chert and clastic rocks associated with the MORB-like basalts represent an accretionary complex generated by scraping off the subducted oceanic crust. They proposed a gradual change in depositional setting upsequence from a distal oceanic environment (lacking terrestrial input) to a continental margin (sourcing clastic sediments). This conclusion is supported by a detailed study of rare-earth elements (REE) in the Cleaverville Formation (Kato et al. 1998: Geochimica et Cosmochimca Acta, 62, 3475–3497).

In contrast to the model of Isozaki et al., Kiyokawa & Taira (1998: Precambrian Research, 88, 109–142) proposed an oceanic island-arc environment for the Cleaverville greenstones and associated rocks. They interpreted their field observations in terms of three volcano-sedimentary cycles — basalt–rhyolite bimodal volcanism followed by chemical sedimentation. However, the geochemical data they presented appear to be inadequate to support their model.

New chemical and Nd-isotope data

As a contribution to the 'North Pilbara' NGMA project†, we investigated the chemistry of Regal Formation greenstones at three localities in the Cleaverville area: south of Karratha; in the study area of Ohta et al. (1996: op. cit.; samples 142495 and 142496; Fig. 30), to cross-check their data; and southeast of their study area. We also investigated the chemistry of mafic dykes in the Cleaverville area.

Cleaverville greenstones

Major- and trace-element analyses were carried out at AGSO by XRF and ICP–MS for 18 samples. To check the quality of the resulting data, selected samples were further analysed by ICP–MS at the University of Queensland and the Institute for Study of the Earth Interior, Misasa, Japan.

† The 'North Pilbara' project, a collaborative undertaking by AGSO and GSWA for the National Geoscience Mapping Accord, supported the work documented herein.

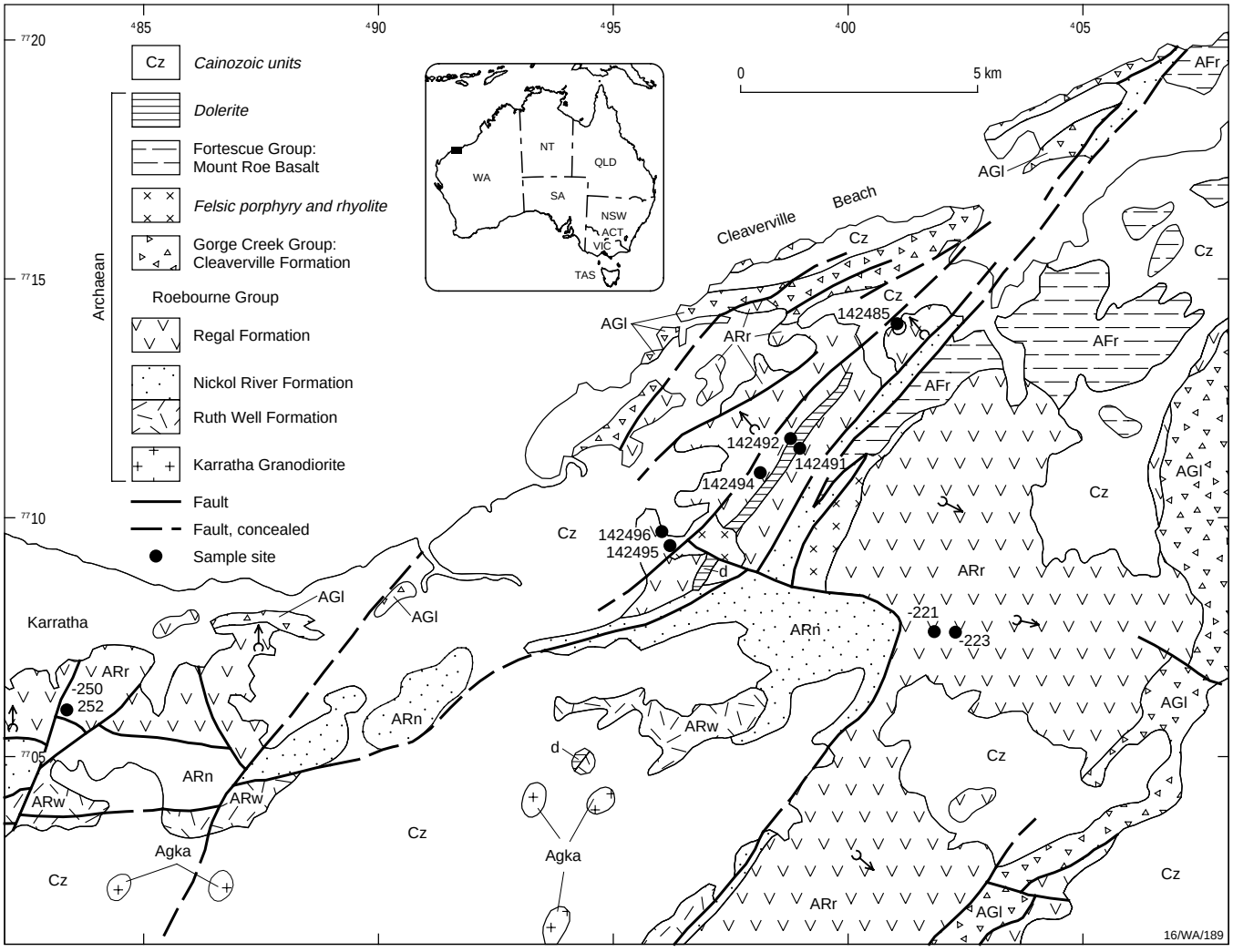

Fig. 30. Simplified geology between Cleaverville and Karratha, west Pilbara, showing Hickman's (1997: op. cit.) revised stratigraphy and sample locations. Note: sample sites annotated '-221', '-223', '-250', and '-252' have the prefix '80040'.

Our new geochemical data (representative samples in Table 2) confirm the MORB-like features of the Cleaverville greenstones (Fig. 31). They show good consistency in Nb/Th (7–8) and Nb/La (0.7–0.9), in marked contrast with the data of Ohta et al. They call into question not only the Nb and Th analyses of Ohta et al. but also the consequential interpretation that the apparent Nb depletion was due to core formation. Furthermore, we suspect that the apparent Fe enrichment relative to pyrolite (estimated for the mantle source of Cleaverville greenstones by Ohta et al.) was due to an increase of MgO as a result of seafloor alteration associated with chlorite formation. Our samples from higher-grade areas do not share this feature.

All samples have slight Nb depletion relative to La, and Th enrichment relative to Nb (Fig. 31). This relative Th enrichment is an atypical MORB character. Unless it is an alteration effect, like Ba, it may instead be due to quicker recycling of crustal material through a subducted zone back into the hotter (100–150°C?) convecting Archaean upper mantle, which is the source region of MORB (e.g., Kerrich et al. 1999: Lithos, 46, 163–187). These MORB-like Cleaverville samples have initial εNd values of +1.0 to +2.5 at 3150 Ma, similar to other early Archaean greenstones.

Northeast-trending doleritic dyke

A mafic dyke (represented by samples 142491, 142492, and 142485) which intrudes the MORB-like basalts is characterised by pronounced light REE and Th enrichment and Nb depletion (Fig. 32). These features are identical with ~2.95-Ga high-magnesian basalts of the Louden Volcanics and Mount Negri Volcanics (sample 331/338 of Sun et al. 1989: in A. J. Crawford, Editor, 'Boninites and related rocks', Unwin Hyman, 148–173). The Louden and Negri Volcanics crop out in the Whim Creek belt (~40–100 km southeast and east of Cleaverville), on the other side of the Sholl Shear Zone (Sun & Hickman 1998: AGSO Research Newsletter 28, 25–28); the distance would have been less than this before post-3020-Ma major sinistral movement along the shear zone.

Sample 142492 has an initial εNd value of –1.5 at 2.95 Ga. This is similar to samples of the Louden and Mount Negri Volcanics, which have initial εNd values of about –2.0 at 2.95 Ga. These initial values are considerably lower than that (~+3) of the depleted mantle at that time and the Cleaverville greenstones. A reasonable explanation for these low initial εNd values, and for the trace-element spidergram patterns of the Cleaverville dolerite dyke and Louden and Mount Negri Volcanics (cf. Fig. 32), is that their mantle source was contaminated by sediments derived mainly from ~3250-Ma source rocks in the region. We suggest that mantle sources of ~3.0-Ga dolerite dykes in the Cleaverville area have been modified by subduction processes (Sun, Nakamura, & Hickman, research in progress). Similarly, geochemical data for basalts in the ca 3.1-Ga Whundo Group (Glikson et al. 1986: op. cit.) south of Cleaverville, across the Sholl Shear Zone, are consistent with juvenile crust generated in a subduction zone environment at this time.

North-trending mafic dyke

A north-trending mafic dyke represented by sample 142494 has intraplate chemical features (Fig. 32). This is similar to the ~2.0?-Ga mafic dyke (sample 86330020) in the Andover Complex, ~20 km to the southeast (Sun & Hoatson 1992: AGSO Bulletin 242, 141–149; Wallace 1992:

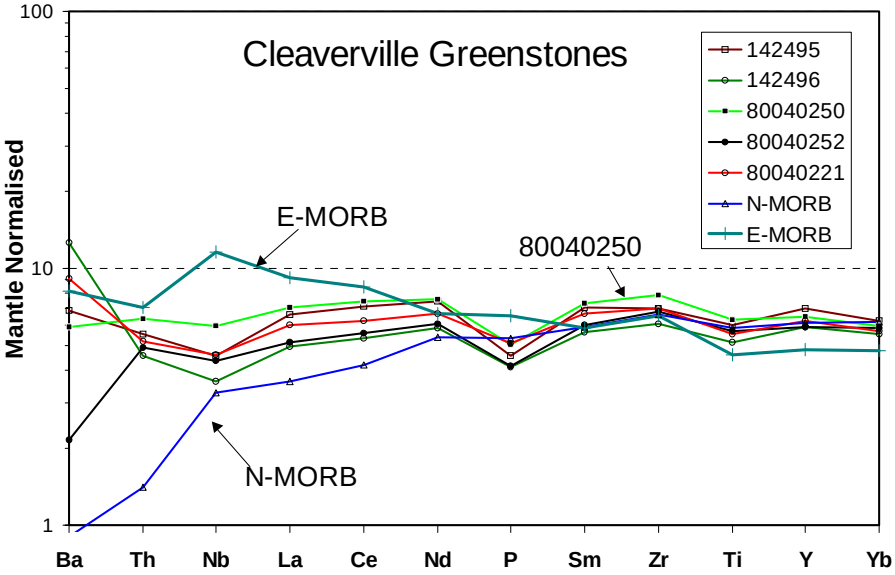

Fig. 31. Mantle-normalised immobile trace-element (except Ba) diagram for MORB-like Cleaverville greenstones. Data of normal mid-ocean-ridge basalt (N-MORB) and enriched MORB (E-MORB) are plotted for comparison.

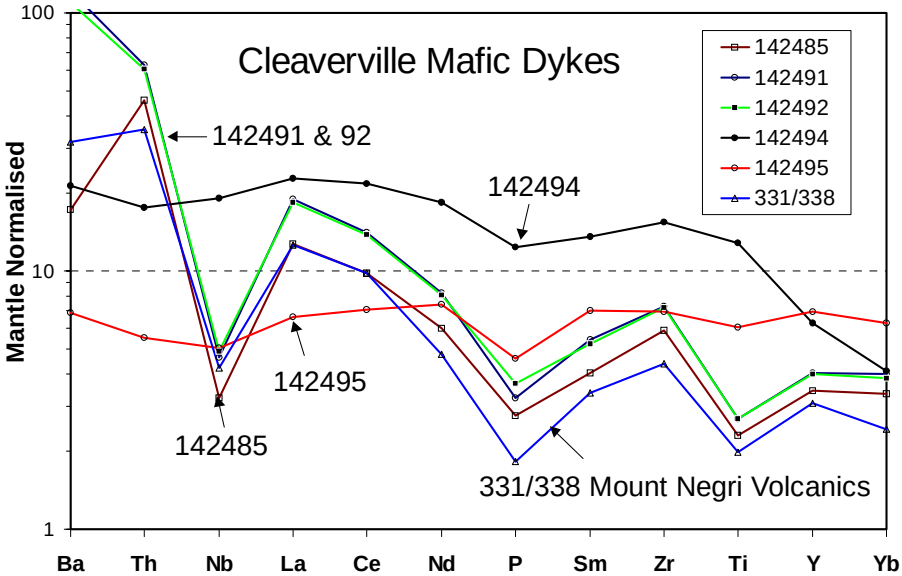

Fig. 32. Mantle-normalised immobile trace-element (except Ba) diagram for ~3.0-Ga Cleaverville dolerite dykes and high-magnesian Louden Volcanics. The pronounced light REE and Th enrichment, and Nb depletion, suggest source modification by subduction zone processes. Sample 142494 (mafic dyke intruding the Cleaverville greenstones) shows intraplate chemical features. A sample (142495) of MORB-like basalts of the Regal Formation is also shown for comparison.

BMR/AGSO Record 1992/13). If these mafic dykes were emplaced at 1850 Ma, samples 142494 and 86330020 would have initial εNd values of +1.6 and +2.2 respectively. Intraplate mafic dykes of this age (~2.0 Ga) may have been generated in response to interaction between the Pilbara and Yilgarn Cratons.

Implications for crustal accretion and tectonic history of the west Pilbara

Our new geochemical data support the view that the Cleaverville greenstone succession of the Regal Formation represents MORB-like oceanic crust overlain by chert–BIF and clastic rocks of the Cleaverville Formation. Away from the Cleaverville–Karratha area, the Regal Formation is not as structurally complex, and evinces no stratigraphic repetition in this basalt–BIF–chert succession. It appears that only at Cleaverville is there sufficient structural complexity to make a case for some type of accretionary complex produced by subduction of the oceanic crust at a continental margin. One of us (Hickman in preparation) believes that the local structural complexity has

Table 2. Chemical composition of mafic igneous rocks of the Cleaverville area and south of Karratha

Sample no.	*142495*	*142496*	*80040221*	*80040223*	*80040250*	*80040252*	*142485*	*142491*	*142492*	*142494*
	Basalt	*Basalt*	*Basalt*	*Basalt*	*Basalt*	*Basalt*	*Dolerite dyke*	*Dolerite dyke*	*Dolerite dyke*	*Dolerite dyke*
SiO2	47.41	48.5	49.6	48.1	50.0	49.3	52.06	53.00	53.6	47.99
TiO2	1.31	1.12	1.20	1.14	1.37	1.24	0.50	0.58	0.58	2.79
Al2O3	14.62	14.52	14.7	15.2	14.9	15.2	13.02	16.06	15.54	12.24
Fe2O3	1.96	1.77	2.46	2.46	1.76	2.37	0.87	1.48	1.93	2.46
FeO	10.17	10.07	10.20	9.75	9.65	10.4	8.42	6.98	6.63	11.94
MnO	0.17	0.16	0.25	0.20	0.2	0.15	0.14	0.13	0.13	0.15
MgO	7.54	7.67	7.00	8.00	7.00	7.50	9.9	5.26	5.13	6.06
CaO	10.28	9.75	10.00	9.65	11.2	8.70	7.28	8.45	8.95	10.32
Na2O	1.85	1.97	2.34	1.86	2.16	3.78	2.97	2.55	2.46	1.88
K2O	0.15	0.21	0.15	0.35	0.06	0.04	0.07	1.75	1.13	0.7
P2O5	0.10	0.09	0.11	0.10	0.11	0.09	0.06	0.07	0.08	0.27
LOI	4.23	3.83	0.94	1.92	0.20	0.20	4.37	3.42	3.54	2.76
Rest	0.15	0.14	0.05	0.10	0.10	0.05	0.23	0.22	0.22	0.17
Total	99.94	99.80	100.02	99.76	99.68	100.05	99.89	99.95	99.92	99.73
Li	16.3	15.6	12.8	23.1	5.4	8.5	22	12.7	11.2	4.3
S	290	680	200	160	481	521	830	180	180	1930
Sc	33	36	40	36	36	40	31	28	30	31
V	288	289	323	304	316	310	179	172	181	330
Cr	136	174	186	139	236		937	173	214	109
Ni	144	140	124	147	111	139	203	89	95	110
Cu	95	99	139	104	104	101	53	58	57	124
Zn	110	101	94	90	83	54	84	76	77	147
Ga			16.6	17.0	16.5	16.5				
Rb	6.7	6.9	5.72	16.3	1.7	0.5	1.7	60.3	35.8	22.5
Sr	185.7	115.2	84.2	100.4	110.4	63	59.9	185.7	160.9	374.7
Y	31.8	26.9	28.5	25.4	29.5	27	15.7	18.4	18.2	28.7
Zr	78	68	78	71	88	76	66	82	82	173
Nb	3.6	2.9	3.3	3.0	4.2	3.1	2.3	3.3	3.5	13.6
Cs	0.14	0.27	0.67	1.02	0.06		0.77	3.15	1.56	6.81
Ba	48	88	64	89	41	15	122	850	765	150
La	4.55	3.41	4.15	3.89	4.82	3.55	8.73	13.00	12.64	15.72
Ce	12.61	9.48	11.14	10.25	13.17	9.90	17.5	25.14	24.48	38.60
Pr	1.9	1.50	1.76	1.60	2.08	1.62	1.99	2.72	2.83	5.35
Nd	10.08	7.90	8.99	8.00	10.31	8.22	8.13	11.09	10.95	25.07
Sm	3.13	2.51	2.95	2.64	3.24	2.68	1.78	2.4	2.31	6.05
Eu	1.14	0.93	1.01	0.96	1.12	1.00	0.58	0.77	0.72	2.17
Gd	3.66	3.15	3.83	3.41	4.09	3.97	2.14	3.87	3.71	6.17
Tb	0.74	0.62	0.70	0.62	0.74	0.71	0.37	0.45	0.44	1.01
Dy	4.82	4.15	4.50	4.00	4.74	4.44	2.38	2.94	2.93	5.55
Ho	1.05	0.93	1.00	0.88	1.03	1.06	0.53	0.65	0.63	1.07
Er	2.89	2.54	2.87	2.56	2.98	3.03	1.47	1.81	1.73	2.49
Tm	0.46	0.39	0.44	0.39	0.47		0.23	0.28	0.27	0.34
Yb	3.09	2.74	2.81	2.49	2.93	2.88	1.65	1.97	1.90	2.02
Lu	0.45	0.39	0.43	0.39	0.45	0.43	0.24	0.29	0.28	0.27
Ta	0.22	0.18	0.27	0.20	0.26	0.27	0.19	0.27	0.27	0.86
Pb	0.83	0.52	1.82	0.95	0.85	0.5	4.70	9.03	8.45	1.67
Th	0.47	0.39	0.44	0.42	0.54	0.42	3.91	5.33	5.16	1.50
U	0.12	0.10	0.11	0.10	0.13	0.10	1.14	1.56	1.51	0.41
Nb/La	0.79	0.85	0.80	0.77	0.87	0.87	0.26	0.25	0.28	0.87
Nb/Th	7.66	7.44	7.50	7.14	7.78	7.38	0.59	0.62	0.68	9.07
Th/U	3.92	3.90	4.00	4.20	4.15	4.20	3.43	3.42	3.42	3.66

another explanation. In terms of Hickman's model, the Regal Formation (with MORB-like basalts) has been thrust across the 3260-Ma units, and — along with the overlying Cleaverville Formation — more likely represents the upper part of an obducted ophiolite.

Subduction zone processes apparently modified the mantle source of ~2.95-Ga mafic rocks over a large area of the northwest Pilbara; similar rocks crop out in the Mallina Basin, southeast of the Whim Creek Belt (Smithies et al. 1999: Precambrian Research, 94, 11–28). The trace-element characteristics of the northeast-trending Cleaverville doleritic dyke and the ~2.95-Ga Louden and Mount Negri Volcanics, such as Nb depletion and Th and Ba enrichment (Fig. 32), may be generated by subduction zone processes. However, an island-arc or cordilleran environment is not essential for the generation of these basalts; rather, many basalts originating in an intraplate environment could have had their mantle source regions modified by prior subduction processes. A closer examination of all pertinent geological information and an integrated interpretation of the data of the Whim Creek Belt and Mallina Basin might reveal the evidence for such processes.

[1] Minerals Division, Australian Geological Survey Organisation, GPO Box 378, Canberra, ACT 2601; tel. +61 2 6249 9484; fax +61 2 6249 9983; email shen-su.sun@agso.gov.au.

[2] Geological Survey of Western Australia, 100 Plain Street, East Perth, WA 6004; tel. +61 8 9222 3220; fax +61 8 9222 3633; email a.hickman@dme.wa.gov.au.

Small-angle neutron scattering

A new technique to detect generated source rocks

Andrzej Radlinski[1]

Despite all its sophistication, geochemistry cannot distinguish source rocks that have generated hydrocarbons from those that merely have the potential to do so. In recent years, in collaboration with neutron scientists in the Oak Ridge National Laboratory (USA) and Institute Laue-Langevin, Grenoble (France), AGSO has developed a new low-cost technique for detecting the invasion of rock pore space during primary hydrocarbon migration, thus enabling the identification of hydrocarbon-generation zones in organic-rich rocks.

Small-angle neutron scattering (SANS) is a routine technique available at neutron-scattering facilities associated with research nuclear reactors. For over 50 years, SANS has been used to study the microstructure of alloys, ceramics, polymers, colloids, and other materials. SANS was preceded by its sister technique of SAXS (small-angle X-ray scattering), and sedimentary rocks (in particular, coals) provided some of the first systems studied with this method.

The early SAXS and SANS results for sedimentary rocks were puzzling and could not be appropriately interpreted owing to the lack of theoretical models for such complex systems. This obstacle was removed in the 1980s with the advent of fractal geometry and pioneering SEM, SANS, and SAXS work on shales, sandstones, coals, and carbonates, which demonstrated that sedimentary rocks are often self-similar on the microscale.

In a typical SANS curve for a hydrocarbon source rock (Fig. 33), the quantity (Q) on the horizontal axis is a measure of the (small) angle between the incident beam and the scattered beam of neutrons. Q is related to the average size, R, of structural features that contribute most to the scattering intensity, I(Q): R = 2.5/Q. On the double-logarithmic scale, the scattering curve approximates a straight line, which is indicative of self-similarity of the rock structure. The pore-size distribution and the internal surface area of the pore space can be readily calculated from such SANS curves.

The SANS technique distinguishes thermal neutrons scattered at the rock–pore space interface. Experimental data can be interpreted to provide specific information about the geometry of the pore space in the range 1 nm to 10 μm, which covers the entire pore-size range for a shale. Typically, the specific internal surface area can be measured and the pore-size distribution quantified.

The intensity of scattering signal depends on the type of fluid present in the pore space. When pores are filled with gases or water, the scattering intensity is high. When the rock becomes invaded with freshly generated bitumen in the process of primary migration, however, the scattering intensity decreases markedly. Such a drop of scattering intensity is a typical SANS signature of hydrocarbon generation in a source rock.

SANS intensity provides an indication of the depth of hydrocarbon generation (Fig. 34). The neutron-scattering intensity measured for a selected value of Q is determined by the scattering properties of the pore-filling fluid. The minimum intensity, at a depth of 3150 ± 50 m, corresponds to pores filled with generated bitumen, thus indicating the position of the hydrocarbon source kitchen.

The SANS method has been tested on artificial rock-like

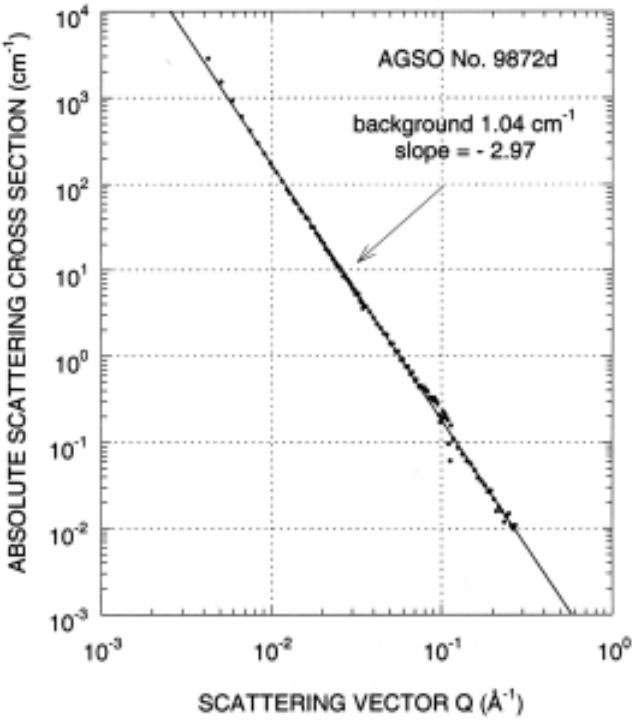

Fig. 33. Plot of absolute SANS intensity versus the scattering vector, Q, for a hydrocarbon source rock.

laboratory preparations, as well as on the artificially and naturally matured series of source rocks. The results have been compared with other geochemical maturity indicators. The process of hydrocarbon generation and associated internal overpressure may lead not only to a decrease in scattering intensity but also to the deformation of pore spaces, which can be readily detected through changes in the scattering intensity pattern. Thus, the value of slope of the scattering curve for a natural maturity series of source rocks reflects the degree of complexity of the pore–rock interface. In Figure 35, for example, it varies from –4 for flat, crystal-like interfaces to –3 for extremely convoluted ones, and the slopes for large pores (small Q-values) and small pores (large Q-values) are different above a particular maturity level owing to pore-space deformation by forced migration of generated hydrocarbons.

SANS is most effective when it is performed in conjunction with Rock-Eval pyrolysis and TOC determination. The cost of commercial SANS analysis is in the mid-range of other geochemical methods.

[1] Petroleum & Marine Division, Australian Geological Survey Organisation, GPO Box 378, Canberra, ACT, 2601; tel. +61 2 6249 9549; email andrzej.radlinski@agso.gov.au.

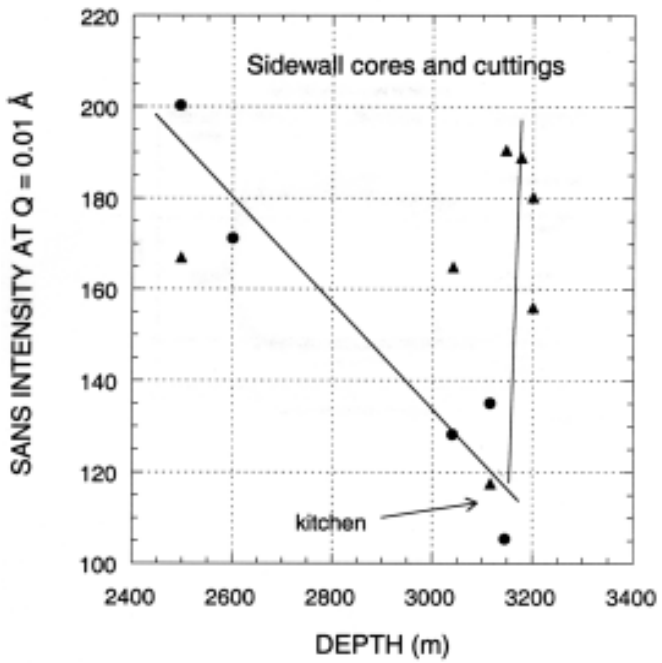

Fig. 34. SANS intensity at the Q-value corresponding to average pore size of 25 nm for a series of potential source rock samples from a recently drilled well on the North West Shelf. Circles correspond to sidewall cores and triangles to cuttings.

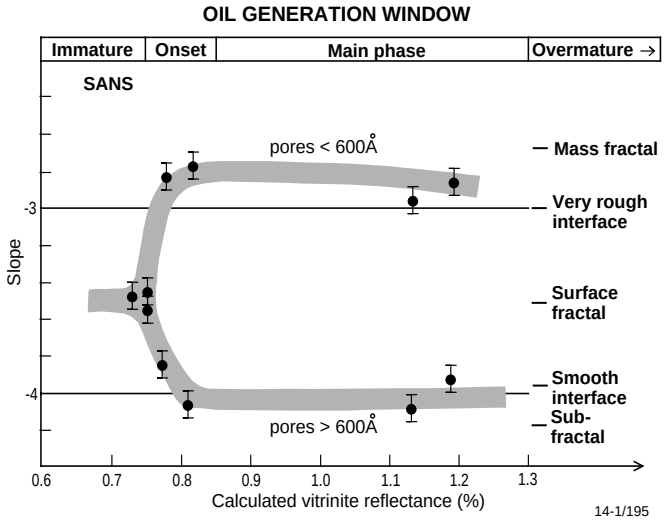

Fig. 35. Slope of the scattering curve versus the value of vitrinite reflectance calculated from the MPI index for a mid-Proterozoic natural-maturity series of source rocks from Urapunga No. 4 well, McArthur Basin (NT).

Tectonic provinces of the Lord Howe Rise

'Law of the Sea' study has implications for frontier hydrocarbons

Howard M.J. Stagg[1], Irina Borissova[1], Mark Alcock[1], & Aidan M.G. Moore[1]

Australia's 200-n-mile Exclusive Economic Zone (EEZ) and 'extended continental shelf' beyond Lord Howe and Norfolk Islands in the Tasman Sea takes in an area of about 1.4 million km², similar to that of the State of Queensland. Despite its vast size and long-term hydrocarbon potential, the Lord Howe Rise region is one of the most poorly known parts of Australia's marine jurisdiction. Recent studies for AGSO's 'Law of the Sea' project, in support of defining Australia's jurisdiction, have provided new insights into the tectonic framework and long-term resource potential of this enormous feature.

The rise extends from the Bellona Trough and Challenger Plateau, west of New Zealand, to southwest of New Caledonia, and lies at water depths generally deeper than 1000 m. It is underlain by continental crust which detached from eastern Australia during the breakup of eastern Gondwana leading to the formation of the oceanic Tasman Basin from 85–52 Ma.

During 1999, 'Law of the Sea' project scientists carried out a framework geological study to provide background information pertinent to the definition of Australia's seabed jurisdiction in this region. Owing to the paucity of geophysical data, the project has made extensive use of satellite gravity data to in-fill the interpretation between widely separated seismic lines. Geological samples are equally sparse, being limited to several Deep Sea Drilling Project (DSDP) holes, drilled in the 1970s and 1980s, and a few samples dredged from the flanks of Lord Howe Rise and Dampier and Norfolk Ridges.

Provinces of the Lord Howe Rise

An important early output from this work has been a map of the major tectonic provinces in the region (Fig. 36) — the first such product for this remote part of Australia's jurisdiction.

The 400–600-km-wide rise consists of four subparallel provinces that extend for much of its length. From east to west, these provinces comprise:

- Shallow, planated, probably Palaeozoic basement of the ***Lord Howe Platform***, overlain by a few hundred metres of mainly Cainozoic siliceous and carbonate oozes. To the east, the basement of the New Caledonia Basin is about 5 km deeper and of uncertain crustal affinity, and the western boundary of the platform is defined by a Cretaceous hinge.
- A ***central rifted province*** characterised by a series of poorly defined basement blocks, normally downfaulted to the west, with 2–4 km of Upper Cretaceous and Cainozoic syn- and post-rift section. This province includes the newly named *Moore Basin* in the south, and the *Faust Basin* in the north.
- A ***western rift province*** separated from the central rift by a broad fault zone across which basement is downfaulted to the west. Basement and water depths are considerably deeper than in the central rift, and the syn- and post-rift sediments are thicker. This province includes the newly named *Monawai Basin* in the south, and the *Capel Basin* in the north. Near Lord Howe Island, the central and western rifts cannot be separated, and the combined rift has been referred to as the *Gower Basin*.
- A ***western bounding complex ridge system*** of continental origin. In the north, the *Dampier Ridge* is separated from the western rift province by the *Lord Howe and Middleton Basins*, which may in part be underlain by highly extended lower continental crust. Farther south, where crustal extension is less extreme, the *Monawai Ridge* forms an intact outer margin to the Monawai Basin.

Regional lineaments of the Lord Howe Rise

Regional crustal lineaments are interpreted to be an important factor in the present-day structural divisions of the Lord Howe Rise region. These lineaments are aligned along two principal trends: northeast–southwest, parallel to the Cretaceous–early Cainozoic Tasman Sea spreading direction; and northwest–southeast, resulting from the late Cainozoic formation of the ridge-and-basin complex between Norfolk Ridge and the Tonga–Kermadec Trench. The northeast–southwest lineaments are particularly important to the structural segmentation of the Lord Howe Rise.

The most prominent of these lineaments extends for about 1800 km northeast from east of Jervis Bay — across the Tasman Sea, Dampier Ridge, Lord Howe Rise, and New Caledonia Basin — as far as the Norfolk Ridge. This lineament (the Barcoo–Elizabeth–Fairway Lineament), has gravity and seismic expression as:

- the boundary between the orthogonal seafloor spreading in the south Tasman Sea and the highly segmented, oblique spreading pattern in the north Tasman Sea;
- an offset in the Dampier Ridge and the major offset between the Lord Howe and Middleton Basins;
- a 130-km offset in the western edge of the Lord Howe Platform, and a commensurate northward narrowing of that province;
- southward termination of the Fairway Trough and Fairway Ridge; and
- a northward constriction, and a corresponding change in structural style, of the New Caledonia Basin.

The northwest–southeast lineaments are mainly restricted to the structural provinces east of Lord Howe Rise, although they may also have overprinted some of the older structuring on the rise. These lineaments are most strongly expressed in the segments of the Vening Meinesz Fracture Zone, north of New Zealand, and by the parallel Cook Fracture Zone, some 600–700 km farther north.

Frontiers of hydrocarbon potential

The possibility of unconventional hydrocarbon resources in the Lord Howe Rise region, in the form of gas hydrates, already has been reported (Exon et al. 1998: PESA Journal 26, 148–158). Our study suggests that these resources may be more widespread than originally envisaged. By identifying sedimentary basins that extend for much of the length of the rise, it also confirms the long-term potential of the region for conventional hydrocarbons. The most prospective areas are the central and western rift provinces of Lord Howe Rise, the eastern flank of the rise adjacent to the New Caledonia Basin, and possibly in the New Caledonia Basin itself, where the sediment thickness exceeds 4 km.

[1] Petroleum & Marine Division, Australian Geological Survey Organisation, GPO Box 378, Canberra, ACT, 2601; tel. +61 2 6249 9343 (HMJS), +61 2 6249 9658 (IB), +61 2 6249 9356 (MA), +61 2 6249 9583 (AMGM); email howard.stagg@agso.gov.au, irina.borissova@agso.gov.au, mark.alcock@agso.gov.au, aidan.moore@agso.gov.au.

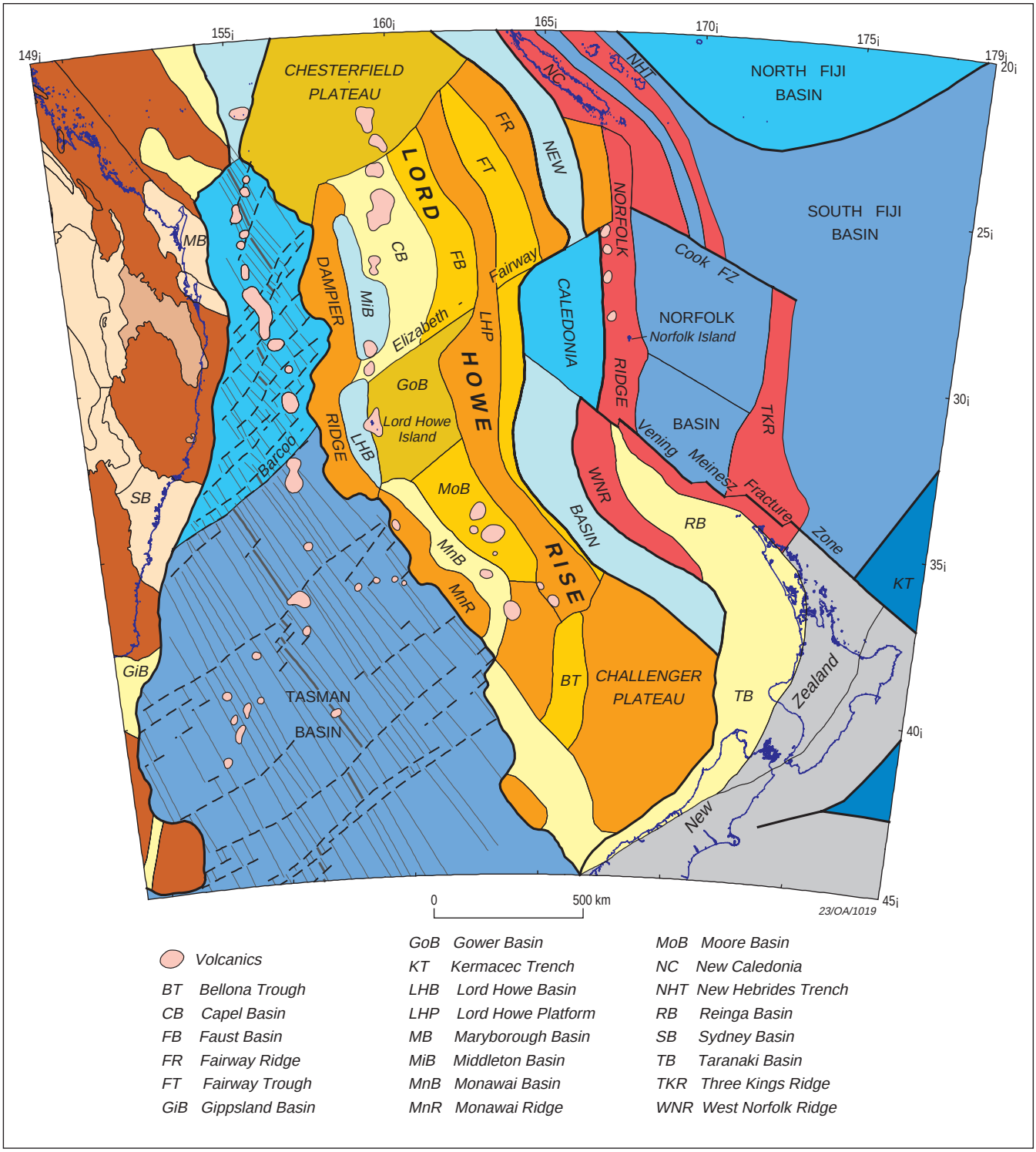

Fig. 36. Structural elements of the Lord Howe Rise region. Blue tones represent ocean basins. On the Australian continent, brown tones represent fold belts; beige, Palaeozoic–Mesozoic basins; yellow, Mesozoic–Cainozoic rift basins. On Lord Howe Rise and ridges to the east, red and deep orange tones represent high-standing basement; yellow, mustard, and pale orange tones, rift-basin elements. New Zealand elements are coloured grey.

The *AGSO Research Newsletter* is published twice a year, in May and November. The camera-ready copy for this issue was prepared by Lin Kay. Correspondence relating to the *AGSO Research Newsletter* should be addressed to Geoff Bladon, Editor, *AGSO Research Newsletter*, Australian Geological Survey Organisation, GPO Box 378, cnr Jerrabomberra Avenue & Hindmarsh Drive, Canberra, ACT 2609; tel. +61 2 6249 9111 (extn 9249) or 6249 9249 (direct), fax +61 2 6249 9984, e-mail geoff.bladon@agso.gov.au. An electronic version of this newsletter is accessible on the WWW at http://www.agso.gov.au/information/publications/resnews/
 ISSN 1039–091X PP255003/00266